Aus dem Lehrstuhl Anatomie II – Neuroanatomie der Anatomischen Anstalt

der Ludwig-Maximilians-Universität München

Vorstand: Univ. Prof. Dr. med. Christoph Schmitz

Immunhistochemische Analyse und Positronen-Emissions-Tomographische Darstellung diffuser Neuroinflammation in murinen Multiple Sklerose Modellen

Dissertation

zum Erwerb des Doktorgrades der Medizin

an der Medizinischen Fakultät der

Ludwig-Maximilians-Universität

vorgelegt von

Anne Theresa Nack

aus Hannover

2021

Mit Genehmigung der Medizinischen Fakultät

der Universität München

Berichterstatter: Prof. Dr. Dr. Markus Kipp

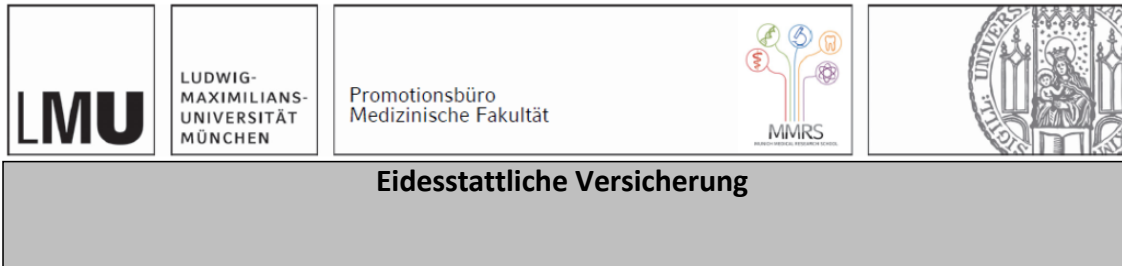Mitberichterstatter: Prof. Dr. Martin Kerschensteiner

                                 PD Dr. Astrid Blaschek

                                 PD Dr. Markus Krumbholz

Mitbetreuung durch den

promovierten Mitarbeiter: Dr. Tanja Hochstrasser

Dekan: Prof. Dr. Thomas Gudermann

Tag der mündlichen Prüfung: 09.12.2021

1. Affidavit

Nack, Anne Theresa

_____

Name, Vorname

Ich erkläre hiermit an Eides statt, dass ich die vorliegende Dissertation mit dem Titel:

**Immunhistochemische Analyse und Positronen-Emissions-Tomographische Darstellung
diffuser Neuroinflammation in murinen Multiple Sklerose Modellen**

selbständig verfasst, mich außer der angegebenen keiner weiteren Hilfsmittel bedient und alle Erkenntnisse, die aus dem Schrifttum ganz oder annähernd übernommen sind, als solche kenntlich gemacht und nach ihrer Herkunft unter Bezeichnung der Fundstelle einzeln nachgewiesen habe.

Ich erkläre des Weiteren, dass die hier vorgelegte Dissertation nicht in gleicher oder in ähnlicher Form bei einer anderen Stelle zur Erlangung eines akademischen Grades eingereicht wurde.

München, 14.12.2021   Anne Theresa Nack

_____   _____

Ort, Datum   Unterschrift Doktorandin bzw. Doktorand

2. Inhaltsverzeichnis

3. Abkürzungsverzeichnis

Abb. – Abbildung

APP – Amyloid precursor protein

Bzw. – beziehungsweise

CNPase – 2,3-zyklische Nukleotid-3-Phosphodiesterase

CT - Computertomographie

EAE – experimentelle autoimmune Enzephalitis

GFAP – glial fibrillary acidic protein

kDa - Kilodalton

MAG – myelin associated glycoprotein

MOG – Myelin-Oligodendrozyten-Protein

MS – Multiple Sklerose

PET – Positronen Emissions Tomographie

PLP – Proteolipid Protein

PPMS – primary progressive Multiple Sclerosis

RRMS – relapsing remitting Multiple Sclerosis

s. Abb. – siehe Abbildung

SPMS – secondary progressive Multiple Sclerosis

TSPO – translocator protein

u. – und

u.a. – unter anderem

ZNS – Zentrales Nervensystem

4. Publikationsliste

1. **Nack A**, Brendel M, Nedelcu J, et al. Expression of Translocator Protein and [18F]-GE180 Ligand Uptake in Multiple Sclerosis Animal Models. Cells. 2019;8(2):94. Published 2019 Jan 28. doi:10.3390/cells8020094

2. Chrzanowski U, Schmitz C, Horn-Bochtler A, **Nack A**, Kipp M. Evaluation strategy to determine reliable demyelination in the cuprizone model. Metab Brain Dis. 2019;34(2):681-685. doi:10.1007/s11011-018-0375-3

5. Einleitung

5.1 Allgemein

Die Multiple Sklerose (MS) ist eine chronisch inflammatorische Erkrankung des Zentralnervensystems (ZNS). Die Inzidenz der MS liegt in Europa und Nordamerika bei über 0,1‰. Allein von 2008 bis 2013 ist die Prävalenz der Erkrankten weltweit um 10% gestiegen (*Atlas of MS*).

Neben Demyelinisierung, Lymphozyteninfiltration und neuronaler Schädigung sind eine Mikrogliose und Astrozytose typische histopathologische Merkmale der Erkrankung. Durch Sekretion von neuronalen Wachstumsfaktoren, Zytokinen und weiteren inflammatorischen Mediatoren verstärken Gliazellen den Entzündungsprozess [1]. Dem pathologischen Verlust der Myelinscheide innerhalb einer entzündlichen Läsion folgt in der Regel eine Remyelinisierung [2].

Klinisch imponieren die entzündlichen Läsionen häufig erstmalig durch Seh- oder Sensibilitätsstörungen. Letztere können je nach Lokalisation der Entzündung an unterschiedlichen Körperregionen auftreten.

Grundsätzlich werden bei der MS drei verschiedene klinische Verlaufsformen unterschieden:

Bei der schubförmig, remittierenden MS (engl. *relapsing remitting*; RRMS) treten einzelne entzündliche Läsionen in Schüben auf. Die Patienten zeigen nach einem Schub einen partiellen oder vollständigen Rückgang der klinischen Symptome. Zwischen den einzelnen Schüben kommt es zu keiner weiteren klinischen Verschlechterung. 80% der Patienten stellen sich initial mit dieser Verlaufsform vor. Anders als bei der RRMS handelt es sich bei den weiteren beiden Arten um progrediente Formen der MS.

Die sekundär progrediente MS (SPMS) entwickelt sich in der Regel aus einer bestehenden RRMS und ist durch eine voranschreitende axonale Schädigung sowie Neurodegeneration gekennzeichnet. Klinisch zeigt sich ein zunehmender Behinderungsgrad, der weitestgehend unabhängig von entzündlichen Schüben auftritt. Die SPMS ist durch diffuse Neurodegeneration sowohl der weißen als auch der grauen Substanz gekennzeichnet.

Die dritte klinische Verlaufsform wird als primär progrediente MS (PPMS) bezeichnet. Ab Beginn der Erkrankung wird eine zunehmende klinische Verschlechterung beobachtet. Diese ist unabhängig von entzündlichen Schüben. Etwa 20% der Patienten sind von der PPMS betroffen.

Während des RRMS-Krankheitsverlaufs dominieren den pathologischen Prozess multifokale entzündliche Läsionen. Bei den beiden progressiven Formen der MS (SPMS, PPMS) beruhen die zunehmenden irreversiblen Behinderungen eher auf diffusen Immunmechanismen sowie Neurodegeneration [3, 4].

5.2 Entstehung und Nachweis diffuser Neurodegeneration

Die Entstehung der diffusen Neurodegeneration ist bisher nicht ausreichend verstanden. Es gibt Hinweise, dass sowohl Mikroglia als auch eingewanderte Monozyten maßgeblich zu den pathologischen Veränderungen beitragen. Histologische Untersuchungen an Gehirnen von MS-Patienten zeigten, dass Mikroglia-Aktivierung nicht nur in Bereichen fokaler Entzündungen, sondern auch diffus in der weißen und grauen Substanz (u.a. *normal appearing white matter)* nachweisbar ist [5].

Mikroglia werden bereits durch kleinste Milieuveränderungen in ihrer Umgebung aktiviert. Bei der Aktivierung spielen auch Astrozyten eine entscheidende Rolle und so ist in Regionen mit ausgeprägter Mikrogliose auch eine Astrozytose nachweisbar [6]. Aktivierte Mikroglia reagieren durch eine vermehrte Ausschüttung von Zytokinen und Chemokinen, vermehrte Phagozytose sowie vermehrte Antigenpräsentierung. Diese Mechanismen könnten maßgeblich zu fortschreitender Neurodegeneration beitragen [7, 8]. Bauer et al. konnten zeigen, dass Mikroglia zusammen mit Makrophagen über Myelin-Phagozytose eine Demyelinisierung bewirken [9].

Die frühzeitige Detektion der Mikroglia-Aktivierung sowie eine Beeinflussung der Funktion könnte also eine entscheidende Rolle für zukünftige Therapieansätze spielen.

Eine etablierte Methode zur *in vivo* Darstellung verschiedener (pathologischer) Prozesse ist die Positronen-Emissions-Tomographie (PET) [10]. Hierbei wird Patienten intravenös ein radioaktiver Marker appliziert, der anschließend mittels spezieller Bildgebung nachgewiesen werden kann. Um Mikroglia-Zellen und somit

diffuse Neurodegeneration nachzuweisen, wurden verschiedene Marker beschrieben. Die bekanntesten Vertreter binden an das mitochondriale 18 kDa *translocator protein* (TSPO). TSPO wird in der äußeren Mitochondrien-Membran exprimiert und ist dort unter anderem für den Cholesterin-Transport essentiell [11]. Weiterhin scheint TSPO eine wichtige Rolle bei der Zellproliferation und Apoptose sowie beim Porphyrin Transport und der Häm-Biosynthese zu spielen [12, 13]. Neben Mikroglia scheinen jedoch noch weitere Zellen im ZNS (insb. Endothelzellen, glatte Muskelzellen, Ependymzellen sowie Astrozyten) TSPO zu exprimieren [14-16].

Bisher verwendete TSPO-Tracer, wie [11C]-PK11195, werden aufgrund eines schlechten Überschreitens der Blut-Hirn-Schranke, schnellem Zerfall und einer unspezifischen Bindung des Liganden im ZNS zunehmend selten verwendet [17, 18]. Neben weiteren Vertretern wurde der TSPO-Ligand [18F]-GE180 entwickelt. Dieser überzeugt durch eine längere Halbwertszeit und einen verbesserten Signal-zu-Hintergrund Kontrast [19]. Bildgebende Studien an MS-Patienten mit diesem Tracer der dritten Generation zeigten bereits gute Ergebnisse [20].

5.3 Tiermodelle

Obwohl es sich bei der MS um eine Erkrankung handelt, die ausschließlich bei Menschen auftritt, repräsentieren präklinische Modelle die histopathologischen Veränderungen hinreichend gut. In den folgenden Arbeiten wurden zwei verschiedene Maus-Modelle sowie eine Kombination aus beiden Modellen verwendet. Die angewandten Modelle unterscheiden sich grundsätzlich voneinander. Beim Cuprizone-Modell führt die Verabreichung eines Kupferchelators zu einer metabolischen Schädigung der Oligodendrozyten, was zu einem progredienten Verlust der Myelinscheiden führt. Eine Infiltration von T-Zellen findet in diesem Modell sekundär statt [21]. Bei der experimentellen autoimmunen Enzephalomyelitis (EAE) handelt es sich um ein (auto)immunes Modell, bei dem eine T-Zell- und Monozyten-Infiltration in das ZNS zu histopathologischen Veränderungen führt [1].

5.3.1 Cuprizone-Modell

Cuprizone ist ein Kupferchelator, der durch oxidativen und metabolischen Stress diffuse histopathologische Veränderungen induziert [22]. Oligodendrozyten reagieren besonders vulnerabel auf Milieuveränderungen, wodurch primäre

Oligodendrozytenschäden entstehen. Diese führen zu einer Aktivierung des angeborenen Immunsystems im ZNS. Eine Einwanderung von Lymphozyten scheint bei der Entwicklung der Cuprizone-induzierten Pathologie keine Rolle zu spielen [1, 21]. Beim Cuprizone-Modell bleibt die Blut-Hirn-Schranke weitestgehend intakt [23].

Cuprizone wird den Tieren über die Nahrung zugeführt. Erstmals beschrieben wurde dieses Verfahren 1966 von William Carlton, der nach der Applikation von Cuprizone eine Demyelinisierung im ZNS beobachtete. In seinen Experimenten wirkte die Applikation von 0,5% Cuprizone toxisch auf die Mäuse, 20% starben vor Beendigung des Experiments. Neben der Demyelinisierung wurden ein vermindertes Größenwachstum sowie das Auftreten eines Hydrozephalus beschrieben [24].

Hiremath et al. erreichten 1998 durch die Cuprizonegabe erstmals reproduzierbare immunhistologische Schädigungen der Myelinscheiden sowie eine deutliche Reduktion der systemischen Toxizität (v.a. Lebertoxizität). Der entscheidende Unterschied zu zuvor beschriebenen Modellen war die Applikation geringerer Cuprizone-Konzentrationen sowie die Verwendung von syngenen Tieren, um eine bessere Vergleichbarkeit zu erzielen. Die Demyelinisierung war leicht induzierbar und die betroffenen Regionen und Ausprägung der Demyelinisierung wurden besser vorhersagbar, weshalb sich dieses Modell für zukünftige Studien durchsetzte. Hierbei wurden 8 Wochen alte C57BL/6 Mäuse über einen Zeitraum von 6 Wochen mit 0,2% Cuprizone gefüttert. Neben der Demyelinisierung wurden im ZNS lokale Entzündungsreaktionen mit Mikrogliose und Astrozytose beobachtet [25].

Der akuten Demyelinisierung folgt in der Regel eine spontane Remyelinisierung [6, 26]. Häufig werden daher zwei verschiedene Varianten des Cuprizone-Modells angewandt. Einerseits werden C57BL/6 Mäuse über 4-6 Wochen mit 0,2% Cuprizone gefüttert und bekommen anschließend normales Futter, um sowohl akute Demyelinisierungs-, als auch Remyelinisierungsstudien durchzuführen. In einem weiteren Modell erhalten die Mäuse das Cuprizone über einen Zeitraum von 12 Wochen, um chronische Demyelinisierungsstudien mit eingeschränkter Remyelinisierung durchzuführen [22].

5.3.2 Experimentelle autoimmune Enzephalomyelitis (EAE)

Die experimentelle autoimmune Enzephalitis ist das am häufigsten angewandte Modell zur Simulation der entzündlichen Prozesse bei der Multiplen Sklerose. Hierbei kommt es zu Inflammation, Demyelinisierung, axonalem Verlust und Gliose [27].

Es existiert eine Vielzahl an unterschiedlichen Protokollen dieses Modells an verschiedenen Säugetieren, die jeweils unterschiedliche klinische, immunologische und histologische Aspekte beleuchten [28]. Grundsätzlich werden bei den meisten Protokollen ZNS-Antigene subkutan oder intrathekal appliziert, wodurch eine Entzündungsreaktion im ZNS entsteht. Der entscheidende Unterschied zum Cuprizone-Modell ist, dass eine primäre T-Zell-Infiltration ins ZNS zu beobachten ist [29].

Keines der EAE-Modelle kann die klinische und histopathologische Komplexität der MS abbilden, verschiedene Teilaspekte können jedoch ausreichend gut durch die Modelle repräsentiert werden. So führt beispielsweise die Applikation von *Proteolipid-Protein* (PLP)$_{139-151}$ in SJL/J Mäusen zu einem schubförmig remittierenden Verlauf, während die Applikation von *myelin oligodendrocyte glycoprotein* (MOG)$_{35-55}$ in C57BL/6 Mäusen zu einem monophasischen chronischen Verlauf führt [30].

Nach der Immunisierung werden die ZNS-Antigene von Antigen-präsentierenden Zellen phagozytiert und gelangen über das lymphatische System zu regionalen Lymphknoten oder zur Milz. In der Peripherie bilden sich daraufhin autoreaktive T-Zellen, die die Blut-Hirn-Schranke überschreiten und in das Parenchym gelangen bzw. über die Blut-Liquor-Schranke in den Liquor und anschließend in das Parenchym gelangen. Hierdurch kommt es innerhalb des Rückenmarks und des Cerebellums zu inflammatorischen Prozessen. Hauptsächlich zeigt sich eine axonale Schädigung, geringer ausgeprägt kommt es zu Demyelinisierung [1]. Klinisch zeigen die Tiere nach 10-14 Tagen eine fortgeschrittene Paraparese. Diese wird regelmäßig mittels eines Scores evaluiert [31].

5.3.3 Kombination: Cup/EAE

Von unserer Arbeitsgruppe wurde ein Modell entwickelt, welches die entstehende Neurodegeneration unter Cuprizone mit der peripheren Immunzellrekrutierung beim EAE-Modell kombiniert (Cup/EAE) [32]. Dabei wird C57BL/6 Mäusen zunächst 3 Wochen lang Cuprizone über das Futter zugeführt. Anschließend bekommen sie über

2 Wochen normales Futter. Hierauf folgt die subkutane Applikation von MOG$_{35-55}$ zur Induktion einer experimentellen autoimmunen Enzephalitis mit Rekrutierung autoreaktiver T-Zellen und Monozyten aus der Peripherie.

In vorherigen EAE-Studien konnte gezeigt werden, dass die Läsionen hauptsächlich im Rückenmark und dem Cerebellum auftreten [26]. Im Cuprizone-Modell hingegen waren Läsionen über das gesamte Cerebrum verteilt zu finden, unter anderem im Hippocampus, Corpus callosum und Kortex. In dem kombinierten Cup/EAE Modell zeigte sich eine signifikant höhere Anzahl an perivaskulären entzündlichen Infiltraten innerhalb des Vorderhirns [33].

5.4 Fragestellung/ Inhalt der Arbeit

5.4.1 *In vivo* Bildgebung diffuser Neurodegeneration

In dem Paper *Expression of Translocator Protein and [18F]-GE180 Ligand Uptake in Multiple Sclerosis Animal Models* war ein Ziel, immunhistologische Veränderungen in murinen MS-Modellen mittels *in vivo* Bildgebung darzustellen und zu überprüfen, inwieweit die bildmorphologische Darstellung mit der tatsächlichen TSPO Expression im Gewebe korreliert. Mittels PET-Scans mit dem TSPO-Liganden [18F]-GE180 wurde im Cuprizone-Modell die TSPO-Ligandenbindung nachgewiesen und anschließend *post mortem* mittels Immunhistochemie mit der TSPO-Expression im Gewebe verglichen. Weiterhin sollte nachgewiesen werden, welche Zellreihen neben Mikroglia TSPO exprimieren. Hierfür wurden immunfluoreszierende Doppelfärbungen angewandt. Im Cuprizone-Modell wurde dargestellt, inwieweit Mikroglia, Astrozyten und Mitochondrien innerhalb geschädigter Axone TSPO exprimieren. Im EAE und Cup/EAE Modell wurde außerdem überprüft, ob TSPO von infiltrierenden Monozyten exprimiert wird.

In der Arbeit konnte bei Cuprizone-behandelten Mäusen eine signifikant höhere Traceraufnahme von [18F]-GE180 im Vergleich zur Kontrollgruppe nachgewiesen werden. Diese zeigte sich in den PET-Scans im Bereich des medialen Corpus callosum ($\Delta 36 \pm 4\%$, $p < 0.001$), des lateralen Corpus callosum ($\Delta 58 \pm 5\%$, $p < 0.001$), des Caudoputamens ($\Delta 65 \pm 5\%$, $p < 0.001$), des Thalamus ($\Delta 47 \pm 5\%$, $p < 0.001$), des Hippocampus ($\Delta 46 \pm 5\%$, $p < 0.001$) und des Cortex ($\Delta 54 \pm 5\%$, $p < 0.001$) (s. Abb. 1).
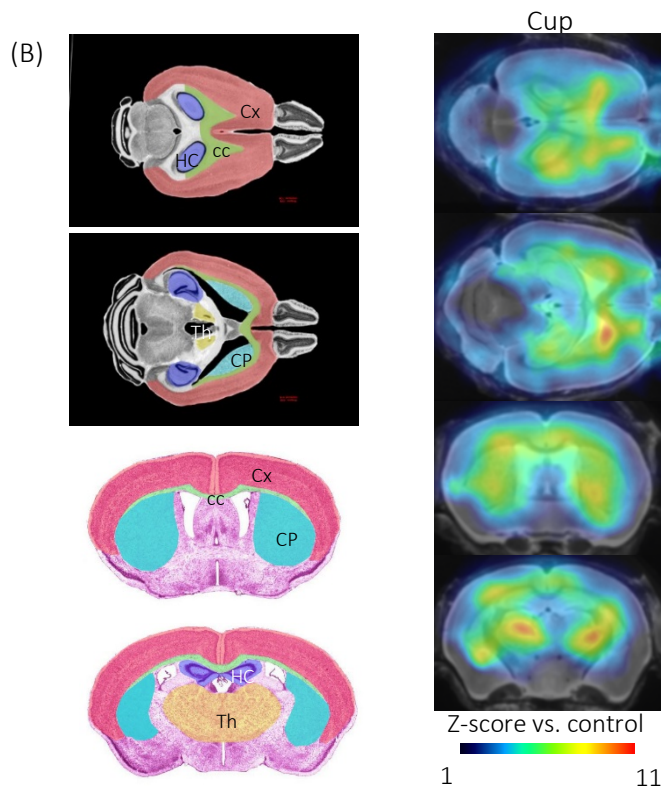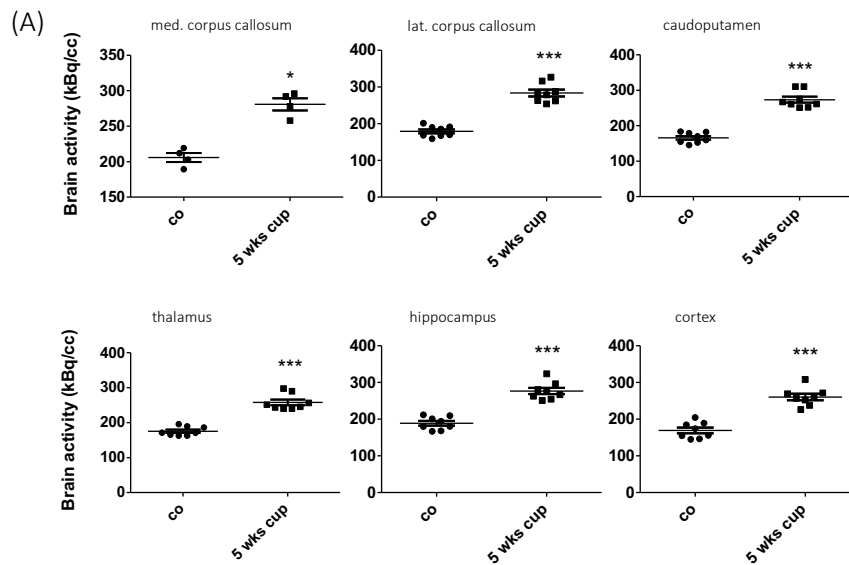
Abbildung 1. *In vivo* Bildgebung zeigt eine erhöhte [18F]-GE180 Aufnahme nach Cuprizone Intoxikation. (**A**) Quantifizierung der Radioliganden-Aufnahme in Kontrolltieren (n=4) im Gegensatz zu einer 5-wöchigen Cuprizone-Intoxikation (n=4). (**B**) Schematische Darstellung der gemessenen Regionen und kumulative *heat map* zur Visualisierung der Ligandenaufnahme in Cuprizone-behandelten Mäusen im Vergleich zu den Kontrollmäusen (Z-Score). (Cx – Cortex, CC – Corpus callosum, HC – Hippocampus, Th – Thalamus, CP – Caudoputamen, Cup – Cuprizone) [34]

Die immunhistochemischen anti-TSPO-Färbungen der Paraffinschnitte wurden mittels densitometrischer Messung und im Cortex mittels manuellen Auszählens der

angefärbten Zellen ausgewertet. Bei den Kontrolltieren war insgesamt eine geringe Färbeintensität nachweisbar. Vereinbar mit den Ergebnissen der PET-Bildgebung zeigte sich bei den Cuprizone-behandelten Tieren eine deutliche höhere Färbeintensität im medialen Corpus callosum ($\Delta 153 \pm 15\%$, $p < 0.001$), dem lateralen Corpus callosum ($\Delta 151 \pm 11\%$, $p < 0.001$), dem Caudoputamen ($\Delta 82 \pm 15\%$, $p < 0.001$), dem Thalamus ($\Delta 35 \pm 6\%$, $p < 0.001$), dem Hippocampus ($\Delta 128 \pm 23\%$, $p < 0.05$) (s. Abb. 2A) und nach manueller Auszählung der angefärbten Zellen auch im Kortex (s. Abb. 2B). Es konnte somit eine gute Korrelation der *in vivo* Bildgebung und den histopathologischen Veränderungen nachgewiesen werden.
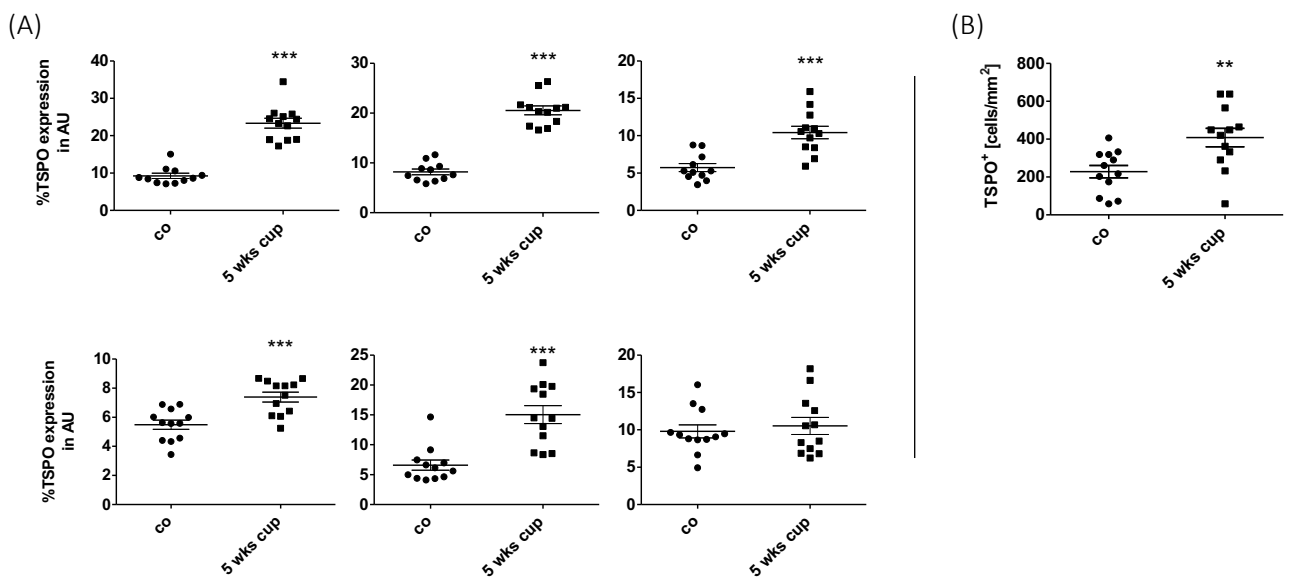

Abbildung 2. (**A**) Densitometrische Quantifizierung der anti-TSPO Färbeintensität in verschiedenen Hirnregionen. (**B**) Quantifizierung anti-TSPO positiver Zellen im somatosensorischen Kortex von Kontrolltieren und nach 5-wöchiger Cuprizone-Behandlung [34].

Für die immunfluoreszierenden Doppelfärbungen wurden jeweils Färbungen mit anti-TSPO und anti-IBA1 zum Nachweis von Mikroglia bzw. anti-GFAP zum Nachweis von Astrozyten durchgeführt. Um herauszufinden, ob TSPO von kumulierenden Mitochondrien innerhalb der axonalen Spheroide von Neuronen exprimiert wird, färbten wir TSPO zusammen mit dem *amyloid precursor protein* APP an.

Insgesamt zeigten 97% der IBA1^{+} Mikroglia, 31% der GFAP[+] Astrozyten und nur 3% der APP[+] axonalen Spheroide eine Kolokalisation mit TSPO (s. Abb. 3 u. 4).
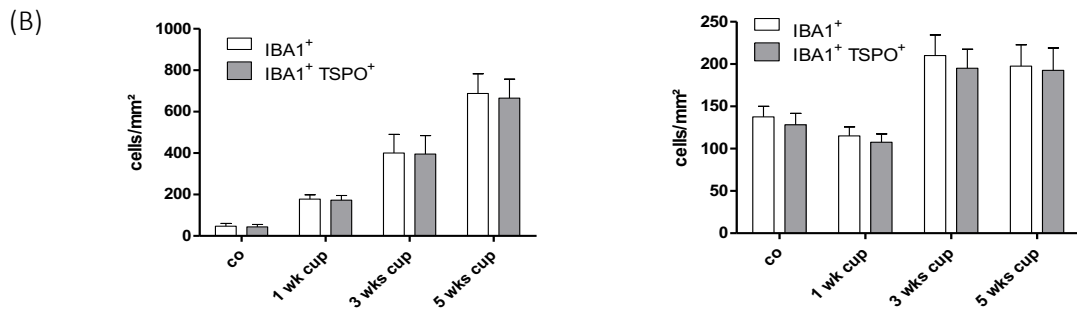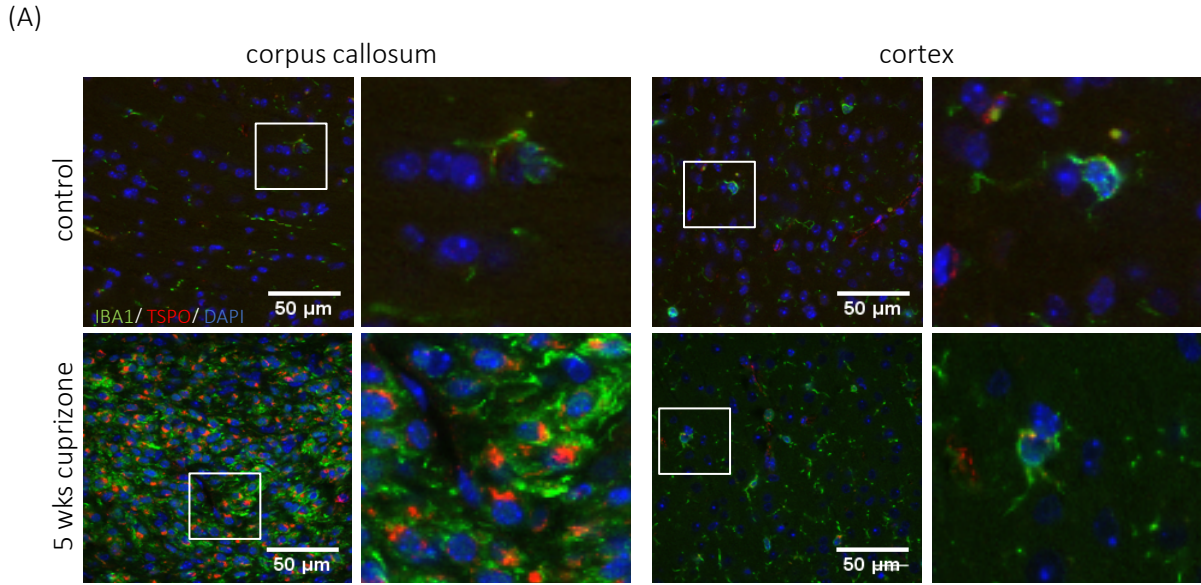
Abbildung 3. Kolokalisation von TSPO und dem Mikroglia-Marker IBA1. (**A**) Immunfluoreszierende Doppelfärbungen von TSPO (rot) und IBA1 (grün) in Kontroll- und Cuprizone-behandelten Mäusen. Die weißen Kästchen kennzeichnen die Areale, die rechts daneben in höherer Auflösung dargestellt sind. (**B**) Quantifizierung der gezählten IBA1+ Zellen und der IBA1+/TSPO+ Kolokalisation bei Kontrolltieren (n=4) und Cuprizone-Intoxikation über 1 (n=5), 3 (n=5) und 5 (n=5) Wochen. (links – Corpus Callosum, rechts – Cortex) [34].

Abbildung 4. Kolokalisation von TSPO und dem Astrozyten-Marker GFAP. Quantifizierung der gezählten GFAP+ Zellen und der GFAP+/TSPO+ Kolokalisation bei Kontrolltieren (n=4) und Cuprizone-Intoxikation über 1 (n=5), 3 (n=5) und 5 (n=5) Wochen. (links – Corpus callosum, rechts – Cortex) [34].
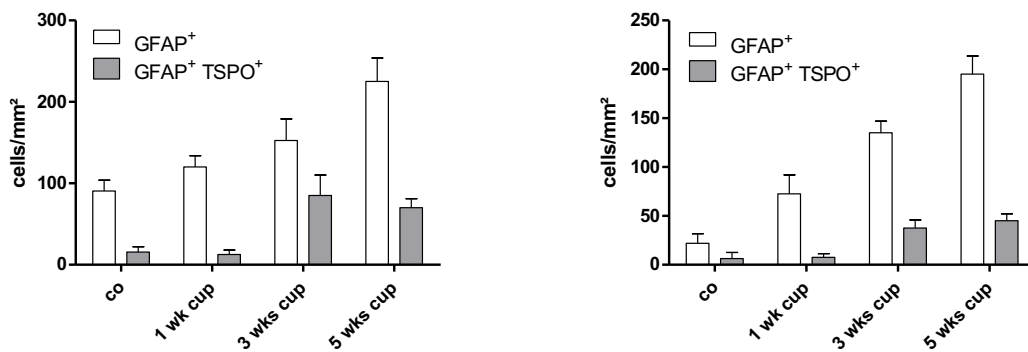
Da die immunpathologischen Veränderungen im Cuprizone-Modell nicht primär auf immunologischen Prozessen beruhen, wurden außerdem MOG-EAE- und Cup/EAE-behandelte Mäuse untersucht. Hier sollte überprüft werden, ob infiltrierende Monozyten ebenfalls TSPO exprimieren. Im MOG-EAE-Modell entstehen die inflammatorischen Prozesse hauptsächlich im Rückenmark und dem Cerebellum. Wie zu erwarten, zeigte sich in diesem Modell im Corpus callosum im Vergleich zu den Kontrolltieren keine signifikant höhere TSPO-Expression. Im Cup/EAE Modell dagegen konnte vor allem um perivaskuläre entzündliche Läsionen im Corpus callosum eine höhere TSPO-Intensität nachgewiesen werden (s. Abb. 5 A, B). Das Cup/EAE Modell wurde an transgenen (CX3CR1+/eGFP/CCR2+/RFP) Mäusen mit RFP-exprimierenden Monozyten und eGFP-exprimierenden Mikroglia angewandt. Hierbei zeigte sich eine Kolokalisation der TSPO-Expression sowohl mit den Mikrogliazellen als auch mit den Monozyten (s. Abb. 5 C, D).
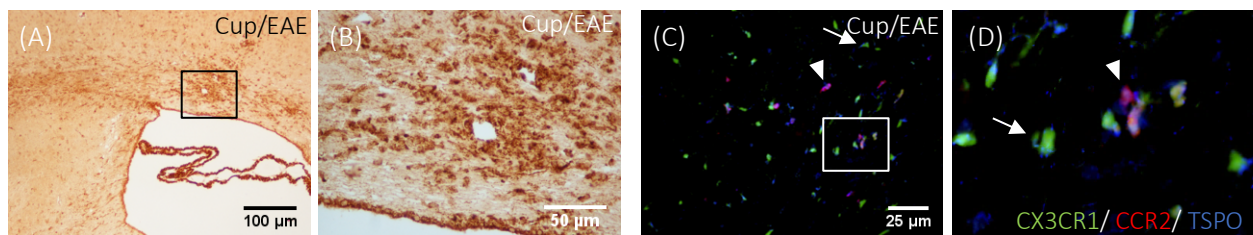

Abbildung 5. (**A, B**) Immunhistochemische anti-TSPO-Färbung in Cup/EAE Mäusen. (**A**) zeigt einen Auschnitt des Corpus callosum mit einer perivaskulären Läsion (schwarzer Kasten), die in (**B**) vergrößert dargestellt ist.
(**C,D**) Corpus callosum von Cup/EAE-behandelten (CX3CR1+/eGFP/CCR2+/RFP) Mäusen. Zu sehen sind Mikroglia (grün), infiltrierende Monozyten (rot) und TSPO (blau). Der weiße Kasten in (**C**) ist in (**D**) vergrößert dargestellt. Die Pfeile zeigen die Kolokalisation von TSPO und Mikroglia, die Pfeilspitzen die Kolokalisation von TSPO und infiltrierenden Monozyten [34].

5.4.2 Strukturierte Demyelinisierungsanalyse im Cuprizone-Modell

Neben der diffusen Neurodegeneration ist die Demyelinisierung ein wichtiger Aspekt der MS. Wie bereits beschrieben folgt der Demyelinisierung in der Regel eine spontane Remyelinisierung. Mittels Cuprizone-Modell können sowohl Demyelinisierungs- als auch Remyelinisierungsprozesse, sowie mögliche Therapieansätze für eine schnellere Remyelinisierung untersucht werden. Ziel der zweiten Publikation war, eine strukturierte Demyelinisierungsstudie im Cuprizone-Modell durchzuführen. Mit der Frage, in welchen Regionen des Corpus callosum eine konstante und nahezu vollständige Demyelinisierung entsteht, sollte eine Grundlage für zukünftige Remyelinisierungsstudien geschaffen werden. Wir verglichen in den Paraffinschnitten drei verschiedene Myelinproteine, die jeweils durch immunhistochemische Antikörperbindungen nachgewiesen wurden (PLP, *myelin associated glycoprotein* [MAG] und *2',3'-cyclic-nucleotide 3'-phosphodiesterase* [CNPase]).

Die Cuprizone-Intoxikation wurde in verschiedenen Gruppen über 1, 3 und 5 Wochen durchgeführt. Die Paraffinschnitte wurden jeweils mit Kontrolltieren verglichen. Untersucht wurde das Corpus callosum auf Höhe des rostralen Hippocampus. Eine Hälfte des Corpus callosum wurde von der Mittellinie ausgehend in 22 Sektoren mit einer Breite von 100μm eingeteilt. Die immunhistochemischen Färbeintensitäten wurden densitometrisch ausgewertet. Es zeigte sich, dass die Färbeintensität bei allen drei angewandten Antikörpern nach einer Woche unverändert blieb. Nach 3 Wochen konnte bei der anti-MAG-Färbung ein signifikanter Rückgang der Intensität im lateralen Bereich des Corpus callosum beobachtet werden. Die anti-PLP- und anti-CNPase-Färbungen blieben nahezu unverändert. Nach der 5-wöchigen Intoxikation zeigte sich ein signifikanter Verlust der anti-PLP-, anti-CNPase- und anti-MAG-Färbeintensitäten vor allem in den mittleren 5 Sektoren (500μm) des Corpus callosum (s. Abb. 6). Zusammenfassend konnten wir also zeigen, dass nach einer 5-wöchigen Cuprizone-Intoxikation die medialen Sektoren des Corpus callosum auf Höhe des rostralen Hippocampus ideal für zukünftige Remyelinisierungsstudien verwendet werden können.
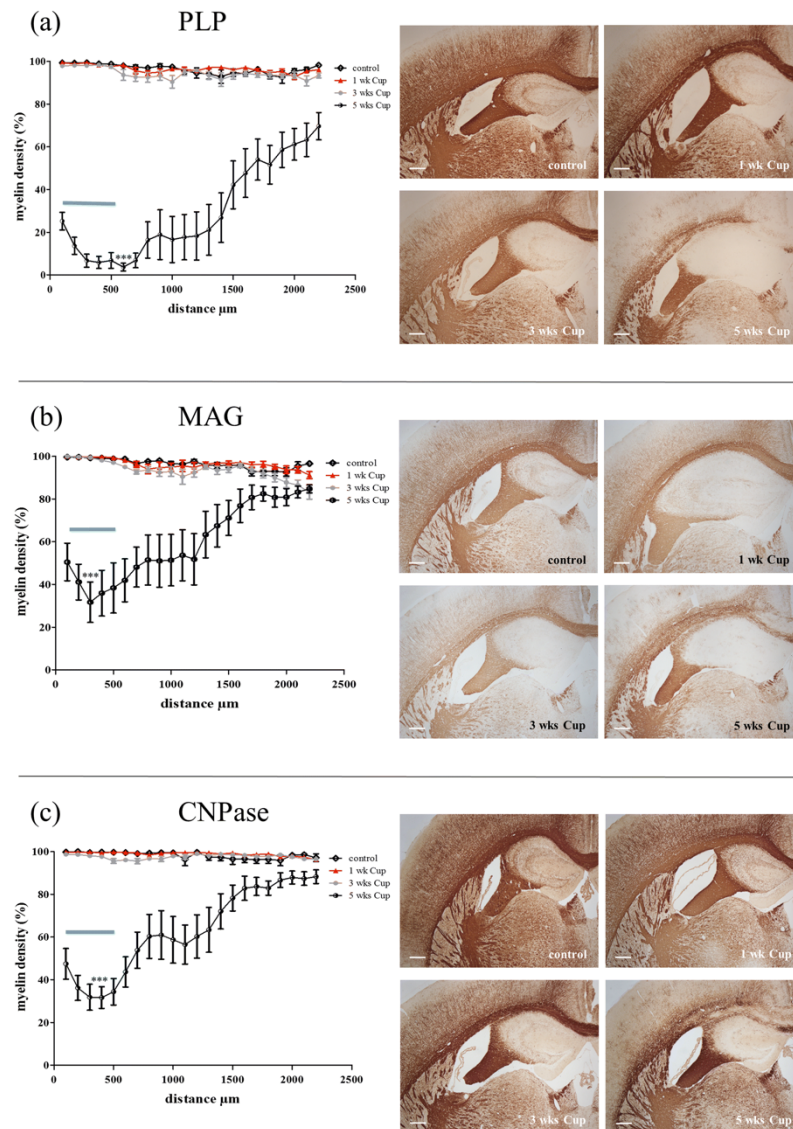
Abbildung 6. (a) Anti-PLP, (b) anti-MAG und (c) anti-CNPase Färbungen im Vergleich nach 1, 3 und 5-wöchiger Cuprizone-Intoxikation. Das Corpus callosum wurde horizontal in 22 Sektoren mit einem Abstand von je 100μm unterteilt, blaue Linie = mediale 500μm ab Mittellinie. Rechts: repräsentative Aufnahmen der Färbungen [35].

5.5 Eigenanteil

Unter Anleitung meines Doktorvaters Univ. Prof. Dr. med. Dr. rer. nat. Markus Kipp führte ich gemeinsam mit der Arbeitsgruppe die Tierhaltung mitsamt Anwendung der verschiedenen Tiermodelle, die Fixierung des Gewebes in Paraffin sowie die immunhistologische Aufarbeitung durch. Weiterhin war ich an der Koordination der Projekte beteiligt.

Für die Publikation „*Expression of Translocator Protein and [18F]-GE180 Ligand Uptake in Multiple Sclerosis Animal Models*" führte die Arbeitsgruppe von Univ. Prof. Dr. med. Axel Rominger die intravenöse Applikation des radioaktiven Liganden sowie die PET Bildgebung mitsamt der Auswertung durch. Da es sich bei der Arbeit um eine Kooperation der Nuklearmedizinischen Klinik Großhadern und des II. Lehrstuhls der Anatomischen Anstalt der LMU handelte, die hauptsächlich von Herrn PD Dr. med. Matthias Brendel und mir durchgeführt wurde, entstand eine geteilte Erstautorenschaft. Meine Eigenleistung beinhaltete die Literaturrecherche, die Anwendung der beschriebenen Immunhistochemie/ Immunfluoreszenz mitsamt der ausführlichen Auswertung. Anschließend wurden die Ergebnisse von mir eigenständig zusammengefasst und in Form der Abbildungen visualisiert. Die gewonnenen Ergebnisse wurden bereits in Form einer Posterpräsentation beim ECTRIMS Kongress 2017 in Paris von mir vorgestellt. Das Manuskript wurde schließlich gemeinsam mit meinem Doktorvater Herrn Univ. Prof. Dr. med. Dr. rer. nat. Markus Kipp und Herrn PD Dr. med. Matthias Brendel eigenständig verfasst.

Für die zweite Publikation belief sich mein Eigenanteil auf die Beteiligung an der immunhistochemischen Färbung mit densitometrischer Auswertung der anti-PLP-Präparate, Beteiligung an der Literaturrecherche sowie das Korrekturlesen der Publikation.

6. Zusammenfassung

Ein Ziel der ersten Publikation war die Darstellung diffuser Neurodegeneration mittels Positronen-Emissions-Tomographie (PET) *in vivo*. Ein Protein, welches bei diffuser Neuroinflammation vermehrt exprimiert wird, ist das *translocator protein* (TSPO). In der Arbeit wurde der TSPO-Ligand [18F]-GE180 sowohl Kontroll- als auch Cuprizone-behandelten Mäusen appliziert und mittels PET visualisiert. Die bildgebenden PET-Daten wurden schließlich mit den histopathologischen Veränderungen in Paraffinschnitten verglichen. Das zweite Ziel war die Identifikation der Zellpopulationen, die hauptsächlich TSPO exprimieren. Hierfür wurden Schnitte Cuprizone-behandelter C57BL/6-Mäuse und transgen veränderter Reporter-Mäuse mittels immunfluoreszierender Doppelfärbungen bzw. anti-TSPO-Färbung analysiert. Neben dem Cuprizone-Modell wendeten wir das EAE-Modell sowie eine Kombination aus beiden (Cup/EAE) an, um experimentell ein Einwandern peripherer Immunzellen zu induzieren und die monozytäre TSPO-Expression zu analysieren.

In der Studie konnte gezeigt werden, dass mittels [18F]-GE180-PET die Cuprizone-induzierte Gliazell-Aktivierung sowohl in Regionen mit weißer Substanz als auch in Regionen mit grauer Substanz (Corpus callosum, Cortex, Hippocampus, Thalamus, Caudoputamen) zuverlässig visualisiert werden kann. Immunhistochemisch zeigte sich neben der vermehrten Gliazell-Aktivierung und TSPO-Expression eine vermehrte Demyelinisierung und axonaler Schaden. Innerhalb der weißen Substanz konnte eine höhere TSPO-Expression als in der grauen Substanz beobachtet werden. Insgesamt exprimierten 97% aller Mikroglia-Zellen sowie etwa ein Drittel der Astrozyten TSPO. Obwohl TSPO in der äußeren Mitochondrienmembran exprimiert wird und in direkter Umgebung von axonaler Schädigung ein Anstieg der Mitochondrienzahl beobachtet werden konnte, war hier keine vermehrte TSPO-Expression nachweisbar. Im Cup/EAE Modell wurde TSPO sowohl von Mikroglia als auch von eingewanderten Monozyten exprimiert.

Zusammenfassend wurde nachgewiesen, dass der TSPO-Ligand [18F]-GE180 verlässlich und reproduzierbar für die *in vivo* Visualisierung neuropathologischer Veränderungen im MS Modell genutzt werden kann. Zellpopulationen, die in den verwendeten MS Modellen TSPO exprimieren sind hauptsächlich Mikroglia, aber auch Astrozyten und eingewanderte Monozyten.

In der zweiten Studie sollten Bereiche mit vollständiger und reproduzierbarer Demyelinisierung im Cuprizone-Modell nachgewiesen werden, um zukünftige Remyelinisierungsstudien zu erleichtern. Für Remyelinisierungsstudien ist die konsistente und komplette Demyelinisierung eine wichtige Voraussetzung. Da die Demyelinisierung im Cuprizone Modell im Bereich des Corpus callosum auf Höhe des rostralen Hippocampus sehr ausgeprägt ist, wurde diese Region untersucht.

Untersuchte Myelin-Proteine waren Proteolipid Protein (PLP), myelin associated glycoprotein (MAG) und 2',3'-cyclic-nucleotide 3'-phosphodiesterase (CNPase). Antikörper gegen diese Proteine wurden in der Studie zum immunhistochemischen Myelinnachweis nach einer jeweiligen Cuprizone-Behandlung über 1, 3 und 5 Wochen verwendet. Eine Hälfte des Corpus callosum wurde von der Mittellinie ausgehend in 22 Sektoren mit einer Breite von je 100μm eingeteilt. Nach einer 5-wöchigen Behandlung konnte mittels optischer Dichtemessungen der Färbeintensitäten ein signifikanter Rückgang der anti-PLP, anti-MAG und anti-CNPase-Färbungen beobachtet werden. In den lateralen Bereichen des Corpus callosum konnte dabei lediglich eine inkomplette Demyelinisierung nachgewiesen werden. In den medialen Bereichen, jeweils 500μm von der Mittellinie entfernt, zeigte sich hingegen eine komplette und konsistente Demyelinisierung. Wir empfehlen daher für zukünftige Remyelinisierungsstudien, diese mediale Region des Corpus callosum zu verwenden.

7. Summary

One aim of the first publication was to visualize diffuse neuroinflammation *in vivo* by positron emission tomography (PET). A good marker for neuroinflammation is the expression of the translocator protein (TSPO). For PET imaging we used the ligand [18F]-GE180 targeting TSPO in cuprizone treated and control mice. The detected signals were then compared to the histopathological changes. Although it is known that TSPO is expressed in the outer mitochondria membrane, it is not yet entirely clear, which cells express TSPO under physiological and pathological conditions. The second purpose of this study was the identification of cell populations that show expression of TSPO. Therefore, sections of cuprizone treated C57BL/6 mice and transgenic reporter mice were analyzed using immunofluorescent double labelling respectively anti-TSPO-staining. Besides cuprizone treated mice we used EAE and Cup/EAE to induce peripheral immune cell recruitment and to assess TSPO expression in monocytes.

[18F]-GE180-PET could be shown as a reliable tool to detect cuprizone-induced glia activation in various white and grey matter regions. The elevated TSPO expression was observed in areas of high glia activation, accompanied by demyelination and axonal injury, such as the corpus callosum, cortex, hippocampus, thalamus and caudoputamen. The expression induction was higher in the white matter corpus callosum compared to analyzed grey matter areas. 97% of the microglia and around one third of the astrocytes expressed TSPO. Although TSPO is known to be expressed by mitochondria, accumulating mitochondria at sites of focal axonal injury do not express TSPO. In Cup/EAE mice TSPO expression could be visualized in microglia and recruited monocytes.

In conclusion, we could show that [18F]-GE180 is a valuable marker for in vivo visualization and quantification of neuropathological changes in the MS brain. Cell types expressing TSPO during experimental demyelination are mainly microglia, but also astrocytes and monocytes.

The aim of the second study was to establish a structured analyzation of cuprizone-induced demyelination in order to facilitate future remyelination studies. For remyelination studies consistent and complete demyelination is an essential pre-

condition. Therefore, we analyzed which parts of the corpus callosum at the level of the rostral hippocampus show reproducible and complete demyelination.

Visualized myelin proteins were proteolipid protein (PLP), myelin associated glycoprotein (MAG) or 2',3'-cyclic-nucleotide 3'-phosphodiesterase (CNPase). Sections were analyzed after 1, 3 and 5 weeks of cuprizone intoxication using anti-PLP, anti-MAG and anti-CNPase antibodies. After outlining the midline of the corpus callosum, one site of the corpus callosum was divided into 22 sectors with a width of 100μm. Sectors were analyzed by measuring optical densities. At week 5, a significant loss of anti-PLP, anti-MAG and anti-CNPase staining intensities was observed in the internal sectors of the corpus callosum. The first five sectors, compromising a distance of 500μm from the midline of the corpus callosum, showed most severe demyelination in all three applied immunohistochemical stains. More lateral located sectors showed incomplete demyelination. Hence, our data suggests focusing on this callosal subregion for future remyelination studies.

8. Veröffentlichungen

8.1 Expression of Translocator protein and [18F]-GE180 ligand uptake in multiple sclerosis animal models

Article

Expression of Translocator Protein and [18F]-GE180 Ligand Uptake in Multiple Sclerosis Animal Models

Anne Nack [1,7,‡], Matthias Brendel [2,‡], Julia Nedelcu [1,7], Markus Daerr [1,7], Stella Nyamoya [1,3,7], Cordian Beyer [3], Carola Focke [2], Maximilian Deussing [2], Chloé Hoornaert [4,5], Peter Ponsaerts [4,5], Christoph Schmitz [1], Peter Bartenstein [2], Axel Rominger [2,6,†] and Markus Kipp [7,*,†]

[1] Department of Anatomy II, Ludwig-Maximilians-University of Munich, 80336 Munich, Germany; A.Nack@campus.lmu.de (A.N.); julia.nedelcu@campus.lmu.de (J.N.); Markus.Daerr@campus.lmu.de (M.D.); stella.nyamoya@rwth-aachen.de (S.N.); Christoph_Schmitz@med.uni-muenchen.de (C.S.)

[2] Department of Nuclear Medicine, University Hospital, LMU Munich, 80336 Munich Germany; Matthias.Brendel@med.uni-muenchen.de (M.B.); Carola.Focke@med.uni-muenchen.de (C.F.); Maximilian.Deussing@med.uni-muenchen.de (M.D.); Peter.Bartenstein@med.uni-muenchen.de (P.B.); Axel.Rominger@insel.ch (A.R.)

[3] Institute of Neuroanatomy, RWTH Aachen University, 52074 Aachen, Germany; CBeyer@ukaachen.de (C.B.)

[4] Laboratory of Experimental Hematology, University of Antwerp, 2000 Antwerp, Belgium; chloe.hoornaert@uantwerpen.be (C.H.); peter.ponsaerts@uantwerpen.be (P.P.)

[5] Vaccine and Infectious Disease Institute (Vaxinfectio), University of Antwerp, 2000 Antwerp, Belgium

[6] Department of Nuclear Medicine, Inselspital, University Hospital Bern, 3010 Bern, Switzerland

[7] Department of Anatomy, Rostock University Medical Center, 18055 Rostock, Germany

[*] Correspondence: Markus.Kipp@med.uni-rostock.de; Tel.: +49-381-494-8401

[†] Axel Rominger and Markus Kipp contributed equally to this work as last authors

[‡] Anne Nack and Matthias Brendel contributed equally to this work as first authors

check for updates

Abstract: Positron emission tomography (PET) ligands targeting the translocator protein (TSPO) represent promising tools to visualize neuroinflammation in multiple sclerosis (MS). Although it is known that TSPO is expressed in the outer mitochondria membrane, its cellular localization in the central nervous system under physiological and pathological conditions is not entirely clear. The purpose of this study was to assess the feasibility of utilizing PET imaging with the TSPO tracer, [18F]-GE180, to detect histopathological changes during experimental demyelination, and to determine which cell types express TSPO. C57BL/6 mice were fed with cuprizone for up to 5 weeks to induce demyelination. Groups of mice were investigated by [18F]-GE180 PET imaging at week 5. Recruitment of peripheral immune cells was triggered by combining cuprizone intoxication with MOG$_{35-55}$ immunization (i.e., Cup/EAE). Immunofluorescence double-labelling and transgene mice were used to determine which cell types express TSPO. [18F]-GE180-PET reliably detected the cuprizone-induced pathology in various white and grey matter regions, including the corpus callosum, cortex, hippocampus, thalamus and caudoputamen. Cuprizone-induced demyelination was paralleled by an increase in TSPO expression, glia activation and axonal injury. Most of the microglia and around one-third of the astrocytes expressed TSPO. TSPO expression induction was more severe in the white matter corpus callosum compared to the grey matter cortex. Although mitochondria accumulate at sites of focal axonal injury, these mitochondria do not express TSPO. In Cup/EAE mice, both microglia and recruited monocytes contribute to the TSPO expressing cell populations. These findings support the notion that TSPO is a valuable marker for the in vivo visualization and quantification of neuropathological changes in the MS brain. The pathological substrate of an increase in TSPO-ligand binding might be diverse including microglia activation, peripheral monocyte recruitment, or astrocytosis, but not axonal injury.

Keywords: multiple sclerosis; cuprizone; TSPO; PET; neurodegeneration

1. Introduction

Multiple sclerosis (MS), an inflammatory disorder of the central nervous system (CNS), is associated with the development of demyelinated plaques, oligodendrocyte destruction and axonal degeneration. These pathological processes are paralleled by the activation of astrocytes and microglia, as well as the recruitment of peripheral immune cells into the central nervous system (CNS) [1,2]. Notwithstanding the traditional focus on white matter tracts as the predominantly affected regions in the CNS of MS patients, demyelination also occurs in various grey matter brain regions [3–5], including the hippocampus [6], neocortex [7], thalamus [5], and caudoputamen [5,8]. MS can present in different clinical courses. Relapsing-remitting MS (RRMS) is characterized by single attacks (also known as relapses) with full or partial recovery. There is minimal to no disease progression during the periods between two relapses. Secondary progressive MS (SPMS) is characterized by an initial RRMS disease course, followed by gradual worsening with or without occasional relapses. During this progressive disease course, progression occurs independent of the relapses. Primary progressive MS (PPMS) is characterized by the progressive accumulation of disability from disease onset. During the RRMS disease course, multifocal inflammatory lesions dominate the pathological process, whereas the gradual accumulation of irreversible disability that characterizes progressive MS seems to result more from diffuse immune mechanisms and neurodegeneration [1,9]. As a result, the currently approved drugs for the treatment of RRMS have marginal or no efficacy in progressive MS without inflammatory lesion activity. The development of effective therapies for progressive MS that prevent worsening, reverse damage, and restore function are a major unmet medical need [9].

The pathogenic cascade(s) underlying neurodegeneration is incompletely understood. Recent data suggest that CNS-resident microglia as well as infiltrating inflammatory monocytes play a key role in neurodegeneration [10,11]. For example, microglia cells together with newly recruited blood-borne macrophages orchestrate a new demyelination process by myelin phagocytosis [12]. Moreover, microglial cells are considered to be the main antigen presenting cell population in the CNS and might therefore play important roles during lymphocyte reactivation [13,14]. In the brains of MS patients, microglial activation is not restricted to the focal inflammatory lesions but also diffusely present in normal appearing white and gray matter areas. Therefore, diffuse microglia activation might be responsible for the diffuse neurodegeneration seen in MS patients [15]. Furthermore, in preclinical MS models acute axonal injury predominantly occurs in regions with pronounced microglia activation [16]. If microglia sense injury, they are rapidly activated and respond by the production of cytokines and chemokines, increased phagocytosis, the release of reactive oxygen species as well as by antigen presentation [17,18]. By these mechanisms, microglia can trigger the activation of neurotoxic pathways leading to progressive neurodegeneration. Manipulation of microglia cell function might, therefore, be a valuable strategy to ameliorate or even prevent neurodegeneration in MS patients, and in consequence alleviate disease progression. However, formal proof that the (prolonged) presence of activated microglia is indeed detrimental in MS remains to be established. Hence, a valid method to measure microglia activation in MS patients is urgently needed.

One of the molecules that is highly expressed by activated microglia is the mitochondrial translocator protein 18 kDa (TSPO), formerly known as the "peripheral benzodiazepine receptor" [19]. TSPO is a receptor that is part of a multimeric complex. This complex includes a voltage-dependent anion channel and an adenine nucleotide carrier and locates to the outer mitochondrial membrane [20]. There, TSPO is believed to play crucial roles in cell physiology and development, as suggested by its sequence conservation from bacteria to humans [21]. Although TSPO is believed to be important for maintaining the mitochondrial membrane potential, this protein is also critically involved in cholesterol transport, making it essential for steroidogenesis [22]. In addition, TSPO plays roles in cellular proliferation, apoptosis and inflammation as well as in porphyrin transport and haem

biosynthesis (see [23,24]) for excellent reviews]. In the CNS, TSPO is thought to be mainly expressed by activated microglia cells, although various other cell types, including endothelial and smooth muscle cells, astrocytes and ependymal cells, were shown to express TSPO [25]. In MS tissues and other CNS disorders, microglia and macrophages are believed to represent the bulk of TSPO^{+} cells [25–27]. However, astrocytes have also been shown to upregulate TSPO expression during CNS injuries [26,28]. In fact, the relative contribution of astrocytes to the global binding of TSPO ligands has been, and still is, a matter of debate [29].

Today, conventional MR imaging (MRI) techniques represent an important step during MS diagnostics and clinical follow-up. It is sensitive in demonstrating focal inflammatory lesions and, to a certain extent, diffuse brain atrophy. However, the widespread diffuse pathology within the normal appearing white matter as well as grey matter pathology, which is often related to microglial activation and neurodegeneration, cannot be reliably detected using conventional MRI [30]. Positron emission tomography (PET) is a sensitive method for visualizing MS-related processes at the molecular level, and is a useful tool to visualize neuroinflammation and the activation of microglia [31]. In contrast to other imaging modalities, PET can visualize cell metabolism in real time, and physiological parameters can be quantified in active disease processes. TSPO is the most widely used target in PET imaging of neuroinflammation. The first successful and now most frequently used TSPO-radioligand is (11C) PK11195 [32]. However, (11C) PK11195 has several disadvantages, including limited brain entrance, a poor signal-to-noise ratio and labelling with the impractically rapid decaying isotope, (11C) [31]. This led to the development of a wide range of second- and third-generation TSPO radioligands, including (18F)-GE180 [33] which indicated good performance in MS patients [34,35].

The cellular source of TSPO expression, and hence TSPO-ligand binding in the CNS of MS patients is not entirely clear. While most studies suggest that TSPO is predominantly expressed by activated microglia cells and in consequence an increase in TSPO ligand binding is interpreted as microglia activation [36–40], various other cell types have been shown to express TSPO as well, including astrocytes [41,42]. The aim of this study was, therefore, to establish the applicability of the third-generation TSPO ligand, (18F)-GE180, to (semi-)quantify glia cell activation and neuroinflammation in a MS mouse model, and to directly correlate ligand binding with TSPO expression. Furthermore, we readdressed which cell types express TSPO after experimental demyelination with a focus on astrocytes, microglia cells and sites of acute axonal injury.

2. Material and Methods

2.1. Animals and Experimental Groups

All in vivo experiments were performed as published previously with minor modifications [43–45]. Eight-week-old C57BL/6 female mice (19–20 g) were purchased from Janvier Labs, Le Genest-Saint-Isle, France. The mice were allowed to accommodate to the environment for at least 1 week prior to the beginning of the experiment. The hGFAP/EGFP transgenic mice [46] were used to visualize entire astrocyte cell bodies and processes. The $CX_3CR1^{+/eGFP}/CCR2^{+/RFP}$-mice with RFP-expressing monocyte-derived macrophages and eGFP-expressing microglia [47] were used to analyze whether TSPO is expressed in microglia and/ or monocytes. Microbiological monitoring was performed according to the Federation of European Laboratory Animal Science Associations recommendations. A maximum of five animals were housed per cage (cage area 435 cm^2). The animals were kept at a 13 h light/11 h dark cycle, with a controlled temperature of 22 $\pm$ 2 °C and 50 $\pm$ 10% humidity, with access to food and water ad libitum. It was assured that no light was used during the night cycle period. Nestlets were used for environmental enrichment. The housing conditions for the PET scanned mice were slightly different, e.g., 12 h light/ 12 h dark cycle and six animals per cage. All experiments were formally approved by the *Regierung Oberbayern* (reference number 55.2-154-2532-73-15). The mice were randomly assigned to the following experimental groups: (A) control (co), the animals were provided a diet of standard rodent chow for the entire duration of the study; (B) cuprizone, the animals were intoxicated

with a diet containing 0.25% cuprizone (bis(cyclohexanone)oxaldihydrazone; Sigma-Aldrich, Taufkirchen, Germany) mixed into ground standard rodent chow for one week (1 wk cup), three weeks (3 wks cup), or five weeks (5 wks cup); (C) Cup/EAE, the mice were intoxicated with the cuprizone diet for the first three weeks, and were then immunized with MOG$_{35-55}$ at the beginning of week six as published previously [43,44]; (D) EAE, the animals received the standard rodent chow for the duration of the study and were immunized with MOG$_{35-55}$ at the beginning of week six.

2.2. EAE and Disease Scoring

EAE scoring was daily performed as published previously [43]. To induce the formation of encephalitogenic T cells, the mice were immunized (s.c.) with an emulsion of MOG$_{35-55}$ peptide dissolved in complete Freund's adjuvant followed by injections of pertussis toxin in PBS (i.p.) on the day of and the day after immunization (Hooke Laboratories, Inc., Lawrence, USA). The disease severity was scored as follows: A score of 1 was assigned if the entire tail dropped over the finger of the observer when the mouse was picked up by the base of the tail; a score of 2 was assigned when the legs of the mice were not spread apart but held close together when the mouse was picked up by the base of the tail, or when mice exhibited a clearly apparent wobbly gait; a score of 3 was assigned when the tail was limp and the mice showed complete paralysis of hind legs (a score of 3.5 is given if the mouse is unable to raise itself when placed on its side); a score of 4 was assigned if the tail was limp and the mice showed complete hind leg and partial front leg paralysis, and the mouse was minimally moving around the cage but appears alert and feeding. A score of 4 was not attained by any of the mice in our study.

2.3. Positron Emission Tomography (PET)—Imaging

All rodent PET procedures followed an established standardized protocol for radiochemistry, acquisition and post-processing [48,49]. In brief, [18F]-GE180 TSPO-PET (10.6 ± 2.1 MBq) with an emission window of 60–90 min p.i. was used to measure cerebral microglial activity by a Siemens Inveon DPET (Siemens, Knoxville, Tennessee). All analyses were performed using PMOD (V3.5, PMOD technologies, Basel, Switzerland). Normalization of the injected activity was performed by the previously validated myocardium correction method [50]. TSPO-PET values, derived from a predefined VOI (volume of interest) set (medial corpus callosum (2.2 mm^3), the lateral corpus callosum (2.9 mm^3), caudoputamen (4.4 mm^3), thalamus (4.4 mm^3), hippocampus (4.4 mm^3), and cortex (6.7 mm^3)) were extracted and compared between groups (co versus 5 wks cup) by a Mann–Whitney test. A visual comparison was performed by the calculation of a standardized Z-score difference map for each cerebral voxel for control versus 5 wks cup. To this end, the average and standard deviation maps were generated for the groups of control and 5 wks cup, and the difference between the control and 5 wks cup average maps was scaled by the standard deviation map of control.

2.4. Gene Expression Studies

The gene expression levels were semi-quantified by real-time reverse transcription-PCR ([qRT-PCR] Bio-Rad, Munich, Germany), using SensiMix Plus SYBR and fluorescein (Quantace, Bioline, Luckenwalde, Germany) with a standardized protocol as described previously by our group [51]. The primer sequences and individual annealing temperatures are shown in Table 1. Relative quantification was performed using the ΔΔCt method. The β-actin expression levels were used as the reference. Gel electrophoresis and melting curves of the PCR products were routinely performed to determine the specificity of the PCR reactions (data not shown). To exclude contamination of the reagents with either RNA or DNA, appropriate negative controls were performed.

Table 1. List of primers used in this study (AT—annealing temperature; bp—base pair length).

	Sense	Antisense	Bp	AT
TSPO1	GCCTACTTTGTACGTGGCGAG	CCTCCCAGCTCTTTCCAGAC	152	60
β-Actin 1	GTACCACCATGTACCCAGGC	AACGCAGCTCAGTAACAGTCC	247	60

2.5. Tissue Preparation

For the histological and immunohistochemical studies, the mice were anaesthetized with ketamine (100 mg·kg^{-1} i.p.) and xylazine (10 mg·kg^{-1} i.p.), and then transcardially perfused with ice-cold PBS followed by a 3.7% formaldehyde solution (pH 7.4). The brains were postfixed in a 3.7% formaldehyde solution overnight, dissected, embedded in paraffin, and then the coronal sections (5 μm) were prepared. For the gene expression studies, after transcardial PBS perfusion, the tissues were manually dissected and cut with a vibratom into 400 μm slices. The hippocampus, corpus callosum and cortex tissues were dissected, and the samples were stored at 0 °C in homogenization tubes filled with 1 mL peqGold TriFast (Peqlab Biotechnologie GmbH, Erlangen, Germany) until further processing.

2.6. Immunohistochemistry

Immunohistochemistry was performed as previously published by our group [43,45]. In brief, the antigens were unmasked with heating in either Tris/EDTA (pH 9.0) or citrate (pH 6.0) buffer if appropriate. After washing in PBS, the sections were blocked in blocking solution (serum of the species in which the secondary antibody was produced) for 1 h. Then, the sections were incubated overnight (4 °C) with the primary antibodies diluted in blocking solution. The primary antibodies used in this study are given in Table 2. The next day, the slides were treated with 0.3% hydrogen peroxide in PBS for 30 min and then incubated with biotinylated secondary antibodies for 1 h followed by peroxidase-coupled avidin-biotin complex (ABC kit; Vector Laboratories, Peterborough, UK). The secondary antibodies used in this study are listed in Table 3. The sections were finally exposed to 3,3'-diaminobenzidine (DAKO, Santa Clara, CA, USA) as a peroxidase substrate as published previously [16]. The negative control sections, without primary antibodies or with isotype antibodies, were processed in parallel to ensure specificity of the staining. The stained and processed sections were digitalized using a Nikon ECLIPSE 50i microscope (Nikon, Nikon Instruments, Düsseldorf, Germany) equipped with a DS-2Mv camera. The open source program, ImageJ (NIH, Bethesda, MD, USA), was used to determine the relative area stained by the anti-TSPO antibodies.

Table 2. List of the antibodies used in this study.

Antigen	Species	Dilution	HIER Method	Purchase Number	RRID	Company
Single stains						
PLP	Mouse	1:5,000	None	MCA839G	AB_2237198	Bio-Rad Laboratories, Inc., Germany
TSPO/PBR	Goat	1:100	Tris/EDTA	ab118913	AB_10898989	Abcam, UK
Iba1	Rabbit	1:5,000	Tris/EDTA	019–19741	AB_839504	Wako, USA
GFAP	Chicken	1:5,000	Citrate	ab4674	AB_304558	Abcam, UK
Double stains						
TSPO/PBR	Goat	1:100	Tris/EDTA	ab118913	AB_10898989	Abcam, UK
GFAP	Mouse	1:400	Tris/EDTA	G3893	AB_477010	Sigma-Aldrich, USA
Iba1	Rabbit	1:2,500	Tris/EDTA	019-19741	AB_839504	Wako, USA
APP	Mouse	1:1,000	Tris/EDTA	MAB348	AB_94882	Millipore, Germany
COXIV	Rabbit	1:500	Tris/EDTA	ab16056	AB_443304	Abcam, UK

27

Table 3. List of the secondary antibodies used in this study.

	Order Number	RRID	Supplier
Rabbit anti-goat IgG	BA-5000	AB_2336126	Vector Laboratories, Burlingame, USA
Goat anti-rabbit IgG	BA-1000	AB_2313606	Vector Laboratories, Burlingame, USA
Goat anti-mouse IgG	BA-9200	AB_2336171	Vector Laboratories, Burlingame, USA
Goat anti-chicken IgG	BA-9010	AB_2336114	Vector Laboratories, Burlingame, USA
Cy3 donkey anti-goat IgG	705-165-147	AB_2307351	Jackson ImmunoResearch Labs
Alexa Fluor 488 donkey anti-rabbit IgG	A21206	AB_2535792	Invitrogen, USA
Alexa Fluor 488 donkey anti-mouse IgG	A21202	AB_141607	Invitrogen, USA

2.7. Immunofluorescence Labeling

For immunofluorescence stains, the sections were rehydrated, unmasked, and blocked in the serum of the species in which the secondary antibodies were raised. The sections were incubated overnight (at 4 °C) with the indicated combination of primary antibodies diluted in blocking solution. The primary antibodies used in this study are listed in Table 2. For double-labelling experiments, the anti-TSPO antibodies were either combined with anti-IBA1 for the detection of microglia/macrophages, or anti-GFAP for the detection of astrocytes. Acute axonal injury was visualized with anti-APP antibodies. After extensive washing, the sections were incubated with a combination of fluorescent secondary antibodies (Table 3). For the staining of cell nuclei, the sections were then incubated with Hoechst 33258 (bisBenzimide H 33258 Sigma Aldrich, Steinheim, Germany; 1:10,000) diluted in PBS. In parallel, the negative controls were performed by first incubating sections with the primary antibodies and subsequently incubating these sections with the "wrong" secondary antibodies to exclude unspecific binding of the fluorescent secondary antibodies to primary antibodies [52]. By incubating the sections with each of the fluorescent secondary antibodies alone, unspecific secondary antibody binding to the tissue itself was excluded. The stained and processed sections were documented using an Olympus BX41-Wi fluorescence microscope station (Olympus, Hamburg, Germany). The software, Stereo Investigator (MBF Bioscience, Williston, ND, USA), was used to determine the number of single and double-positive cells/spheroids.

2.8. Ultrastructural Analysis via Serial Block-Face Scanning Electron Microscopy

Myelinated and demyelinated corpora callosa (i.e., 3 wks cuprizone) were analyzed by 3D EM as published by Ohno and colleagues [53]. To this end, the mice were perfused via the left ventricle with 2.5% (wt/vol) glutaraldehyde and 4% paraformaldehyde. The brains were subsequently removed, stained with heavy metals, and embedded in resin. 3D-electron microscopy (Serial block-face scanning EM) was performed by using a SigmaVP scanning electron microscope (Carl Zeiss) equipped with a 3View in-chamber ultramicrotome system (Gatan). Serial image sequences were generated at 80 nm-nm steps, providing 204.54 μm × 61.36 μm-wide image stacks at a resolution of 0.001 μm per pixel. The images were processed and measured with the open source program, Reconstruct (BU, Boston, MA, USA). The focus of this analysis was to detect mitochondria within axonal swellings.

2.9. Statistical Analysis

All data are given as arithmetic means ± SEMs. A *p*-value of <0.05 was considered to be statistically significant. Statistical analyses were performed using Prism 5 (GraphPad Software Inc., San Diego, CA, USA). Applied statistical tests are given in the respective figure legends.

3. Results

3.1. Cuprizone Intoxication Induces Reproducible Demyelination and Glia Activation

First, we analyzed the spatial distribution of cuprizone-induced demyelination and glia activation after a 5-week cuprizone intoxication protocol. Compared to the control animals, severe loss of anti-PLP staining intensity was evident in several brain regions, including the corpus callosum, grey matter cortex

and caudoputamen (see Figure 1A). At the level of the anterior commissure, demyelination of the corpus callosum was prominent at the lateral parts, whereas, at the level of the rostral hippocampus, the medial corpus callosum was most severely demyelinated. Moreover, moderate but consistent demyelination was observed in the hippocampus. To analyze the extent of microglia and astrocyte activation, anti-IBA1 and anti-GFAP immunohistochemical stains were performed, respectively. As shown in Figure 1B, C, demyelination was paralleled by severe microgliosis and astrocytosis. Anti-IBA1 and anti-GFAP staining intensity was most severe within the demyelinated corpus callosum, less so in the affected grey matter cortex and hippocampus. Within the caudoputamen, microgliosis and astrocytosis were severe within the demyelinated striosomes, and moderate in the matrix region.
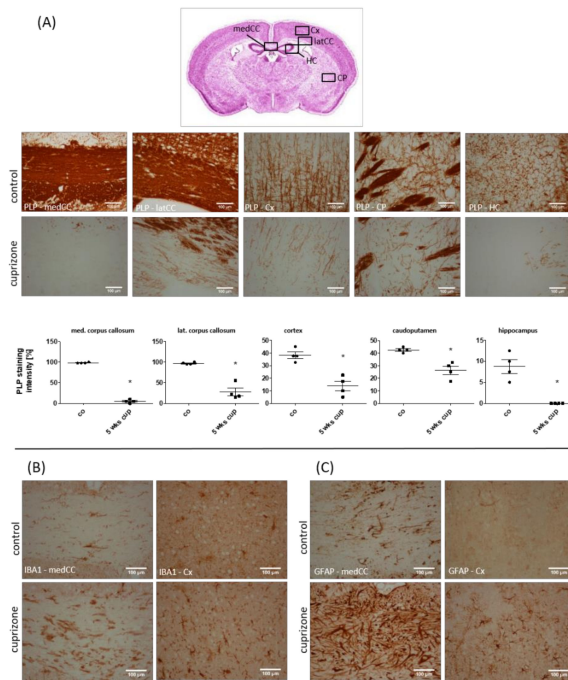
Figure 1. Cuprizone-intoxication induces multifocal demyelination and reactive glia activation. (**A**) The myelination of different brain areas, determined by anti-PLP staining. The upper row shows representative pictures of the control (*n* = 4), and the lower row shows representative pictures of the cuprizone-intoxicated animals (5 weeks; *n* = 4). (**B**) Cuprizone-induced demyelination is paralleled by microglia activation (shown with IBA1 immunoreactivity; *n* = 4), and (**C**) astrocyte activation (shown with GFAP immunoreactivity; *n* = 4). medCC (medial part of the corpus callosum); latCC (lateral part of the corpus callosum); Cx (cortex); CP (caudoputamen); HC (hippocampus). Differences were determined using Mann–Whitney tests. * $p < 0.05$, ** $p < 0.01$, and *** $p < 0.001$.

3.2. TSPO Expression and (18F)-GE180 Uptake Correlate with the Degree of Demyelination and Glial Cell Activation

Different cell types have been discussed to induce TSPO expression in response to brain injuries, including microglia and astrocytes. During inflammatory demyelination, a third cell type might contribute to the global brain TSPO load, namely, recruited monocytes. In a first step, we applied the reductionistic cuprizone demyelination model where demyelination occurs despite the presence of an intact blood–brain barrier, and, in consequence, the absence of peripheral monocytes and

lymphocytes [54]. In that model, we performed µPET analyses in control and 5-week cuprizone-treated animals to quantify uptake of the novel TSPO ligand, (18F)-GE180 [55], and compared ligand uptake to histopathological changes.

In line with previous results [41,56], we found a region-dependent increase of [18F]-GE180 uptake in cuprizone-treated mice (Figure 2A). A visual interpretation of the TSPO µPET scans indicated increased tracer uptake, particularly in the corpus callosum, caudoputamen, thalamus and cortex regions (Figure 2B). Statistical comparison between the control and cuprizone-intoxicated mice showed significant higher tracer uptake in the medial corpus callosum ($\Delta 36 \pm 4\%$, $p < 0.001$), the lateral corpus callosum ($\Delta 58 \pm 5\%$, $p < 0.001$), the caudoputamen ($\Delta 65 \pm 5\%$, $p < 0.001$), the thalamus ($\Delta 47 \pm 5\%$, $p < 0.001$), the hippocampus ($\Delta 46 \pm 5\%$, $p < 0.001$), and the cortex ($\Delta 54 \pm 5\%$, $p < 0.001$).
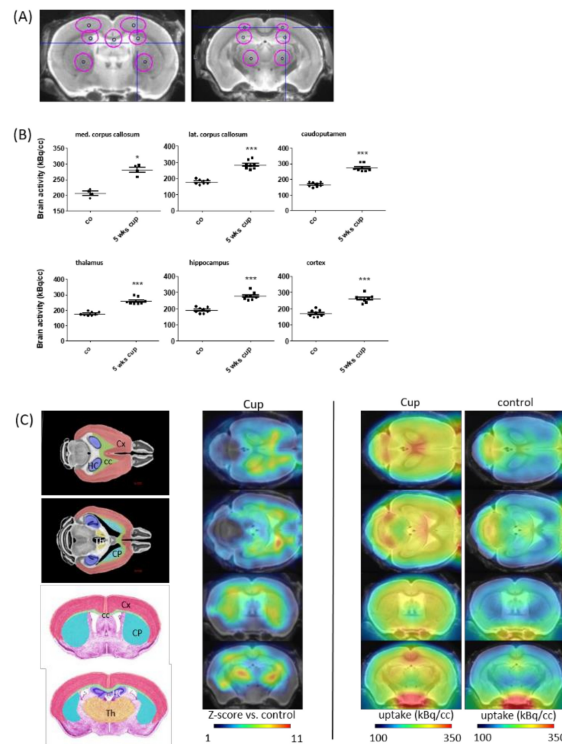

Figure 2. In vivo imaging demonstrates an increase in [18F]-GE180 uptake after cuprizone-intoxication. (**A**) The definition of VOIs (volumes of interest), demonstrated in a mouse brain MRI atlas in the coronal slides: medial corpus callosum (2.2 mm^3), lateral corpus callosum (2.9 mm^3), caudoputamen (4.4 mm^3), thalamus (4.4 mm^3), hippocampus (4.4 mm^3), and cortex (6.7 mm^3). (**B**) The quantification of radioligand uptake in the control animals ($n = 4$) and after a 5-week cuprizone intoxication period ($n = 4$). (**C**) Schematic illustration of the measured areas and cumulative heat map illustrating radioligand uptake in cuprizone-treated mice. The color codes demonstrate the standardized radioligand uptake levels relative to the controls (Z-scores; left column), and the normalized uptake in cuprizone-treated (middle column) and control (right column) mice. Cx (cortex); CC (corpus callosum); HC (hippocampus); Th (thalamus); CP (caudoputamen). Differences were determined using Mann–Whitney tests. * $p < 0.05$, ** $p < 0.01$, and *** $p < 0.001$.

In order to relate the observed increased tracer uptake in vivo to the histological changes, we analyzed TSPO reactivity in the different brain regions. In control animals, the anti-TSPO staining intensity of the brain parenchyma was generally weak. Consistent with the reported mitochondrial localization of the TSPO protein, the quality of the staining was punctate [25]. Due to the punctate nature of the cell processes, complete cell shapes could not easily be deciphered. In line with previous observations, the positive immunohistochemical staining for TSPO was cytoplasmatic [57]. Occasionally, positively-stained process-bearing cells were identifiable as glial cells (arrow in Figure 3A), resembling either microglia or astrocytes. Furthermore, TSPO-expressing cells with multiple processes that appeared to be oligodendrocyte progenitor cells were found in the cortex (see Figure 3B). No staining was observed if the primary antibody was omitted (not shown). Additional cells/areas in which TSPO immunoreactivity was observed in the control brains included cekks in the subpial glia (probably both astrocytes and microglia; arrows in Figure 3C), meninges, ependymal cells (arrows in Figure 3D), as well as cells in the choroid plexus (vessels, macrophages, and choroid plexus epithelial cells; see Figure 3E). TSPO+ cells, resembling oligodendrocytes, were also observed (arrows in Figure 3F). Again, the staining pattern in these cells tends to be punctate or granular. Furthermore, neuronal cell bodies were labelled with punctuate spots (not shown). The brains of cuprizone-intoxicated mice displayed staining in compartments observed in the control cases (such as in the meninges, neurons and ependymal cells), but also showed markedly enhanced staining in the parenchyma, particularly in regions of demyelination such as the corpus callosum (see Figure 3G–I). In such areas of intense demyelination, ramified glial cells had enhanced TSPO positivity, most of which were clearly identifiable as activated microglia (see Figure 3J/K). TSPO+ hypertrophic astrocytes were also present in the brains of cuprizone-intoxicated mice, identified based on their morphology (arrows in Figure 3L).
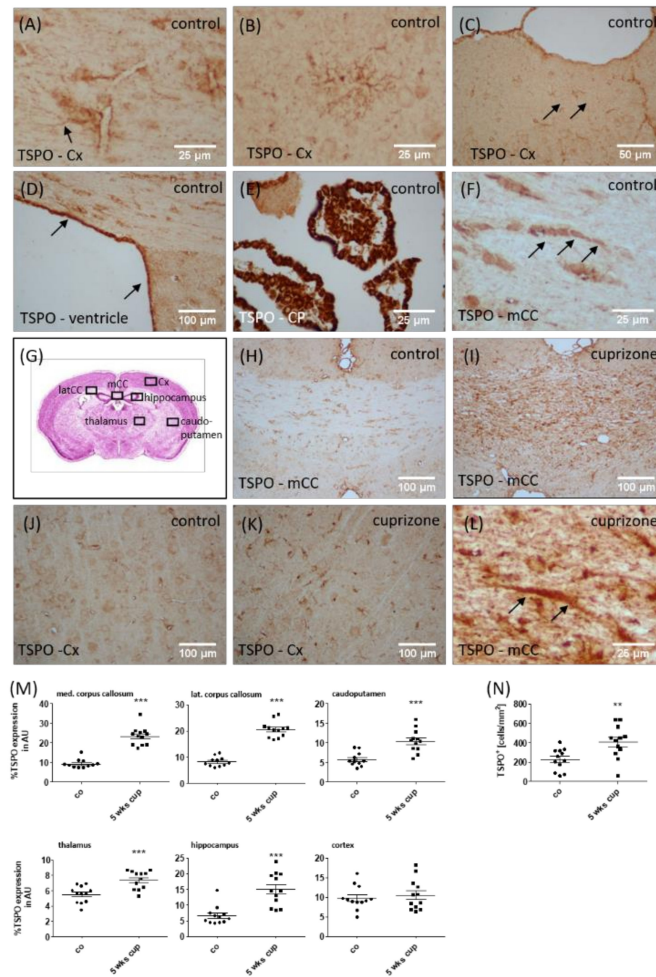
Figure 3. Expression of TSPO in cuprizone-intoxicated mice. The representative results of the anti-TSPO immunohistochemistry demonstrating the expression of TSPO in perivascular astrocytes (arrow in **A**), oligodendrocyte progenitor cells (**B**), glia cells beneath the pial surface of the cortex (**C**), ependymal cells lining the lateral ventricles (**D**), choroid plexus cells (**E**) and interfascicular oligodendrocytes in the corpus callosum (arrows in **F**). (**G**) Schematic illustration of the investigated regions. (**H–K**) The representative results of the anti-TSPO immunohistochemistry in the control or cuprizone-intoxicated mice. (**L**) A high-power view of an anti-TSPO$^+$ astrocyte (arrows) in the corpus callosum of cuprizone-intoxicated mice. (**M**) The densitometric quantification of the anti-TSPO staining intensity in different brain areas. (**N**) The quantification of anti-TSPO$^+$ cell densities in the somatosensory cortex of control and 5-week cuprizone-intoxicated mice, with representative pictures shown in (**J**) and (**K**). mCC (medial part of the corpus callosum); Cx (cortex); CP (choroid plexus). Differences between the groups were statistically tested using two-tailed *t*-test. Welsh correction was applied for the medial corpus callosum. * $p < 0.05$, ** $p < 0.01$, and *** $p < 0.001$.

The densitometrical quantification of TSPO staining intensity revealed significantly higher expression levels in the medial ($\Delta 153 \pm 15\%$, $p < 0.001$) and lateral ($\Delta 151 \pm 11\%$, $p < 0.001$) corpus callosum, caudoputamen ($\Delta 82 \pm 15\%$, $p < 0.001$), thalamus ($\Delta 35 \pm 6\%$, $p < 0.001$) and hippocampus ($\Delta 128 \pm 23\%$, $p < 0.05$), but not in the cortex region. Due to the discrepancy of cortical TSPO expression based on immunohistochemical evaluation, and in vivo µPET analyses, we additionally quantified the densities of TSPO+ cells in the cortex of the control and cuprizone-intoxicated mice, which is a more sensitive method to detect subtle expression differences. As shown in Figure 3N, higher densities of TSPO+ cells were found in the cortex of the cuprizone-intoxicated mice compared to the control mice. To verify induced TSPO expression in the cuprizone model, we quantified *Tspo* mRNA expression by rt RT-PCR in the corpus callosum and cortex after 1, 3 and 5 weeks of cuprizone intoxication. As demonstrated in Figure 4, higher *Tspo* expression levels were found in both the white matter corpus callosum and grey matter cortex region. Additionally, the extent of *Tspo* mRNA expression induction was greater in the corpus callosum compared to the cortex.
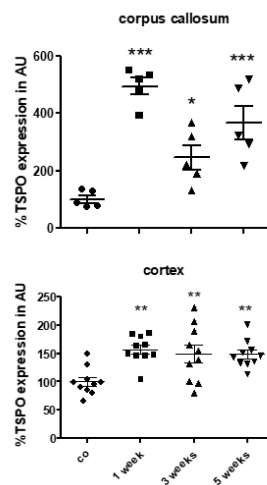

Figure 4. Expression levels of *Tspo* mRNA during the course of cuprizone-induced demyelination. *Tspo* mRNA levels in the control animals ($n = 5$) and the animals intoxicated with cuprizone for one ($n = 5$), three ($n = 5$) or five ($n = 5$) weeks. Differences between the groups were statistically tested using one-way ANOVA with the obtained p-values corrected for multiple testing using the Dunnett's post-hoc test; * $p \leq 0.05$, ** $p \leq 0.05$, *** $p \leq 0.001$.

3.3. TSPO Mainly Co-Localizes with Microglia

As stated above, based on their morphology, TSPO+ cells were identifiable as glial cells, resembling either microglia or astrocytes. Furthermore, it has been suggested that both activated astrocytes and microglia are responsible for the enhanced TSPO-ligand binding in brain areas undergoing cuprizone-induced demyelination [41,58]. To test for this, IBA1/TSPO and GFAP/TSPO double-labelling experiments were performed, and absolute glial cell densities as well as numbers of glia cells expressing the respective glia cell marker protein and TSPO (IBA1+/TSPO+ or GFAP+/TSPO+) was evaluated in the white matter corpus callosum and grey matter cortex after 1, 3 and 5 weeks of cuprizone intoxication. As shown in Figure 5, the densities of the IBA1+ cells gradually increased in the corpus callosum during the course of cuprizone-induced demyelination. At week 5, the mean density of the IBA1+ cells in the medial corpus callosum was 687.5 ± 300.75 cells/mm². Most of the IBA1+ cells also expressed TSPO (665 ± 291.82 cells/mm²; ~97%). In line with previous results [59], the extent of microgliosis was less severe and delayed in the cortex (control: 137.5 ± 35.35 cells/mm²

versus 5 weeks of cuprizone: 197.5 ± 80.325 cells/mm^2). Comparable to what we found in the corpus callosum, most of the IBA1$^+$ cells in the cortex expressed TSPO at week 5 (192.5 ± 84.2 cells/mm^2; ~97%). The situation for GFAP expressing cells was different. Although the densities of the GFAP$^+$ cells gradually increased in the corpus callosum and cortex during the course of cuprizone-induced demyelination, a significant proportion of the GFAP$^+$ cells were TSPO-negative in the control and cuprizone-exposed mice (see Figure 6). At week 5, ~31% of GFAP$^+$ astrocytes co-expressed TSPO in the white matter corpus callosum, whereas ~23% of GFAP$^+$ astrocytes co-expressed TSPO in the grey matter cortex. To verify TSPO expression in the astrocytes, the brain slides from the cuprizone-treated hGFAP-eGFP-mice were processed for anti-TSPO immunoflourescence staining. These mice express eGFP not only in proximal processes, but also in the fine distal processes of astrocytes [46]. In line with our results that were obtained by fluorescence-double-labelling, the anti-TSPO signal could clearly be localized to the astrocyte cell bodies (see Figure 6C).
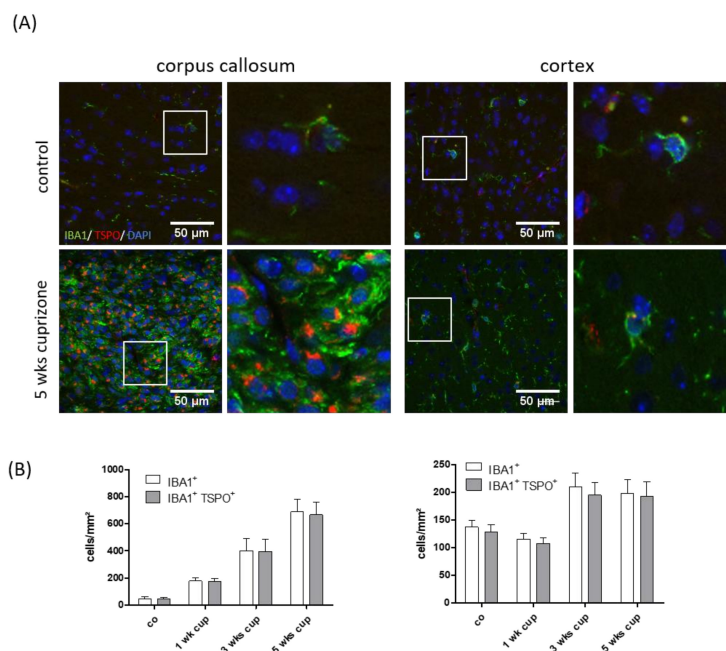

Figure 5. Co-localization of TSPO with the microglia/monocyte marker, IBA1. (**A**) The representative images of IBA1 (green) and TSPO (red) immunofluorescence double stains in the control and 5-week cuprizone-intoxicated mice (left: corpus callosum; right: cortex). The white boxes highlight cells which are shown on the right-hand side at higher magnification. (**B**) The quantification of entire IBA1$^+$ cell densities (white columns) and IBA1$^+$/TSPO$^+$ double positive cell densities (grey columns) in the control animals ($n = 4$) and the animals intoxicated with cuprizone for one ($n = 5$), three ($n = 5$) or five ($n = 5$) weeks.
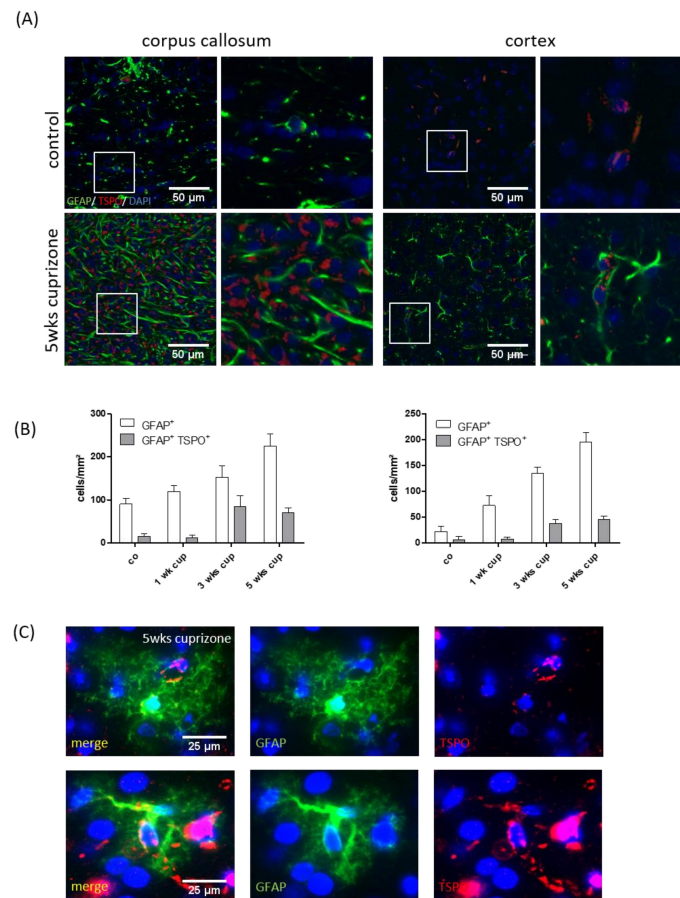
Figure 6. Co-localization of TSPO with the astrocyte marker protein, GFAP (**A**). The representative images of GFAP (green) and TSPO (red) immunofluorescence double stains in the control and 5-week cuprizone-intoxicated mice (left: corpus callosum; right: cortex). The white boxes highlight cells which are shown on the right-hand side at higher magnification. (**B**) The quantification of the entire GFAP$^+$ cell densities (white columns) and GFAP$^+$/TSPO$^+$ double positive cell densities (grey columns) in the control animals (n = 4) and the animals intoxicated with cuprizone for one (n = 5), three (n = 5) or five (n = 5) weeks. (**C**) The representative images demonstrating expression of TSPO (red) in eGFP-expressing astrocytes (green).

3.4. TSPO Is Not Expressed in the Mitochondria of Injured Axons

Different groups reported an increase in mitochondrial content (through an increase in size and number) within demyelinated axons in MS as well as following experimental demyelination [53,60,61]. Therefore, increased (18F)-GE180 binding levels might principally also be due to an increase in the axonal mitochondrial load. To test for this possibility, we first used 3D-electron microscopy to observe the accumulation of mitochondria in the corpus callosum of cuprizone-exposed mice. As expected, numerous mitochondria were found in astrocytes (arrowheads in Figure 7A) and myelin-laden microglia cells (arrowheads in Figure 7B). Some mitochondria were also present in normal-appearing,

myelinated axons (arrowheads in Figure 7C). Additionally, pronounced mitochondrial accumulation was frequently found at sites of axonal swelling (arrowheads in Figure 7D). 3D reconstruction of serial blockface scanning 3D EM images revealed that in many cases, axonal mitochondrial density was high at the close vicinity of an axonal swelling, but continuously declined with increasing distance to the swelling (data not shown).
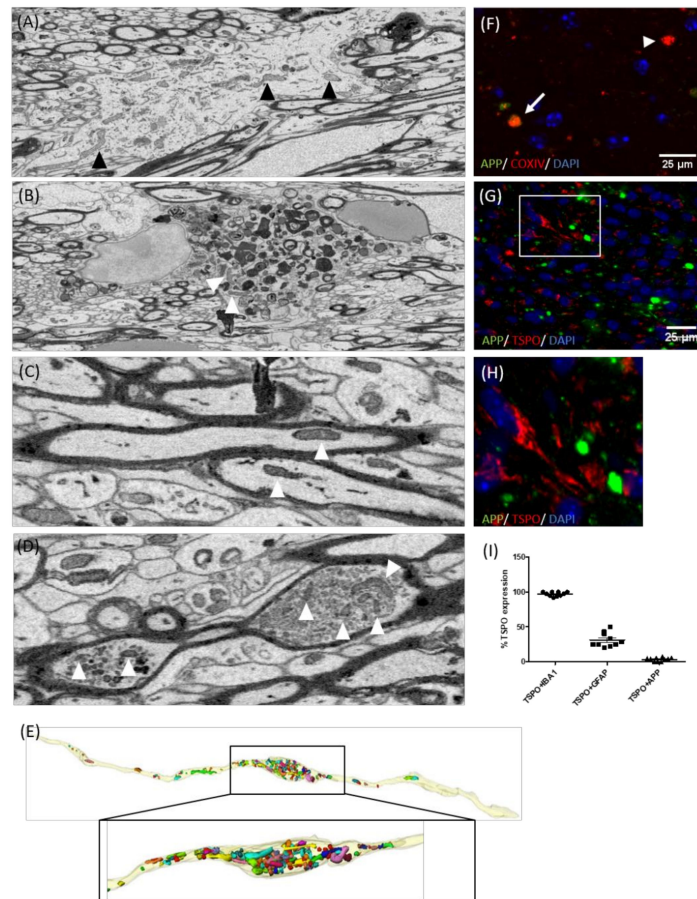

Figure 7. Accumulation of mitochondria in the damaged axons. The representative electron microscopic images demonstrating mitochondria (arrowheads) in the astrocytes (**A**), phagocytosing microglia (**B**), myelinated axons (**C**), or axonal swellings (**D**). The mice were intoxicated with cuprizone for three weeks (*n* = 4). The arrowheads highlight mitochondria. (**E**) 3D reconstruction of an axonal swelling. The mitochondria are highlighted by different colors. (**F**) The representative image of APP (green) and COXIV (red) immunofluorescence double stains in the 5-week cuprizone-intoxicated mice. The arrowhead highlights a COXIV$^+$ single-positive, and the arrow highlights a COXIV$^+$/APP$^+$ double-positive spheroid. (**G**) The representative image of APP (green) and TSPO (red) immunofluorescence double stains in the 5-week cuprizone-intoxicated mice. The white box highlights a region which is shown in (**H**), at higher magnification. (**I**) The percentage of microglia (IBA1$^+$), astrocytes (GFAP$^+$) or axonal spheroids (APP$^+$) co-expressing TSPO.

To verify the ultrastructural data, the presence of mitochondria in axonal spheroids was additionally visualized by APP/COXIV double-labelling experiments. As demonstrated in Figure 7F, most of the APP$^+$ spheroids contained COXIV$^+$ mitochondrial profiles. Next, we looked for the co-labelling of APP$^+$ axonal spheroids with TSPO. Surprisingly, almost no TSPO$^+$/APP$^+$ spheroids were found in the corpus callosum of cuprizone-treated mice (Figure 7I). In particular, ~97% of IBA1$^+$ microglia cells, ~31% of GFAP$^+$ astrocytes, but just ~3% of APP$^+$ axonal spheroids co-expressed TSPO, ruling out that increased [18F]-GE180 binding is due to mitochondrial accumulation within axons.

3.5. TSPO Is Expressed by Both Microglia and Monocytes in Inflammatory Lesions

The results from most studies suggest that cuprizone-induced pathology is characterized by intense microglia accumulation [62], whereas peripheral immune cells have negligible significance for cuprizone-induced demyelination. This reductionist model therefore does not allow the study of TSPO expression of invading monocytes under demyelinating conditions. As recently published by our group [43,44], the combination of cuprizone intoxication and MOG$_{35-55}$ immunization (i.e., Cup/EAE) results in significant peripheral immune cell recruitment. We took advantage of this model to investigate the expression of TSPO in peripheral immune cells (see Figure 8A for the experimental setup). MOG-EAE and Cup/EAE mice showed clinical signs of disease progression beginning ~11 days after immunization, with the Cup/EAE-treated mice reaching slightly higher cumulative (9.38 ± 1.14 versus 7.75 ± 1.05) and maximum (3.0 ± 0.2 versus 2.5 ± 0.35) disease scores than MOG-EAE-treated mice (see Figure 8B). In line with our results described above, a significant increase in anti-TSPO staining intensity was observed in the corpus callosum of only cuprizone-treated mice (Figure 8D). In MOG-EAE mice, no significant increase in anti-TSPO staining intensity could be observed in the corpus callosum (Figure 8E). However, in some cases, perivascular foci were in direct vicinity of the third ventricle, and these foci showed pronounced TSPO immunoreactivity (Figure 8F). In Cup/EAE mice, the TSPO staining intensity was pronounced in the cuprizone vulnerable regions, such as the corpus callosum (Figure 8G). A particularly high TSPO staining intensity was observed around perivascular inflammatory lesions (Figure 8H,I). To determine whether microglia or recruited monocytes express TSPO in the Cup/EAE model, we utilized transgenic (CX$_3$CR1$^{+/eGFP}$/CCR2$^{+/RFP}$) mice with RFP-expressing monocyte-derived macrophages and eGFP-expressing microglia [47]. As shown in Figure 8J,K, the TSPO signal clearly co-localized to both, eGFP-expressing microglia (arrow) and RFP-expressing monocyte-derived macrophages (arrowhead).
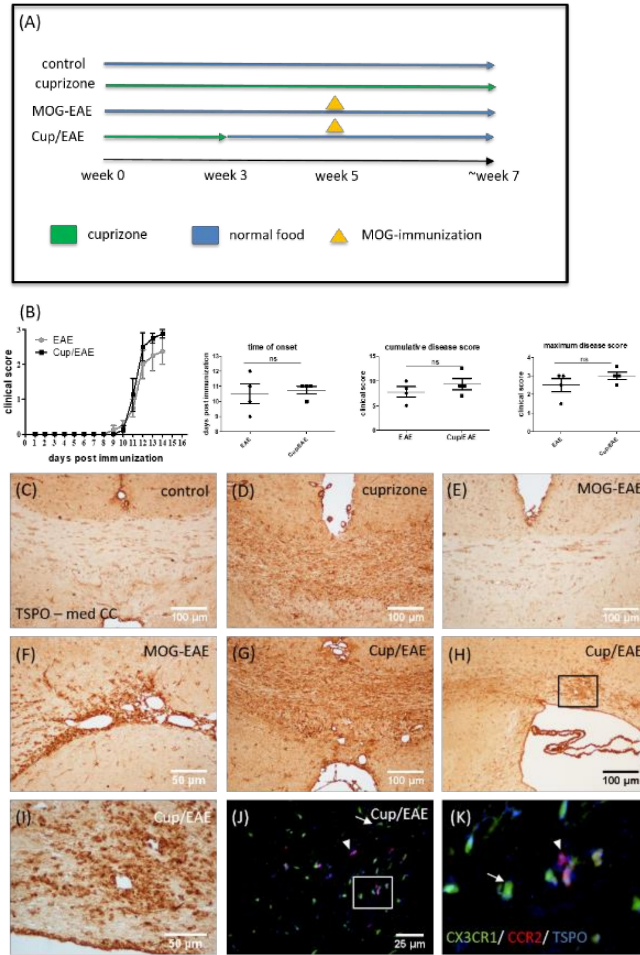
Figure 8. Expression of TSPO in Cup/EAE mice (**A**). Schematic depicting the experimental setup. The periods of normal chow diet are highlighted in blue. The periods of cuprizone intoxication are highlighted in green, and the time point of MOG_{35-55} immunization with subsequent active EAE development are highlighted in orange. (**B**) The clinical scores for MOG-EAE and Cup/EAE treated mice with the time of onset, cumulative disease score and maximum disease score (*n* = 4). The representative images of anti-TSPO immunohistochemistry in the controls (**C**), cuprizone-intoxicated (**D**), MOG-EAE (**E**,**F**), and Cup/EAE (**G**–**I**) mice. The perivascular lesion, highlighted in (**H**) by the black box, is shown in (**I**) at higher magnification. (**J**,**K**) The representative images of the corpus callosum from cuprizone-treated mice, showing microglia (green), infiltrating monocytes (red) and TSPO (blue). The arrow indicates TSPO expression in microglia cells, and the arrowhead indicates TSPO expression in invaded monocytes.

4. Discussion

The present study demonstrates the temporal, regional and cellular patterns of TSPO expression during the progression of cuprizone-induced demyelination in the mouse brain. Furthermore,

this study indicates a very good applicability for monitoring neuroinflammatory processes using the third-generation TSPO radioligand, (18F)-GE180. To the best of our knowledge, this is the first study investigating cuprizone-intoxicated mice using (18F)-GE180 PET with the aim of quantifying the uptake/binding in various anatomical brain regions, and correlating ligand uptake with TSPO expression.

During the last two decades, the prototypic TSPO radioligand in use has been (11C)-PK11195, with the first human brain studies conducted in patients with Rasmussen's encephalitis [63], with glioma [64], and in healthy controls and MS patients [32]. Using (11C)-PK11195 results in increased binding in MS lesions, as demonstrated by postmortem studies and in vivo PET [29,65]. Although (11C)-PK11195 showed promise as a biomarker in MS [66], newer TSPO-selective radioligands might be superior to (11C)-PK11195 based on their higher brain uptake and more specific binding [67]. In this study, we were able to demonstrate that cuprizone-induced demyelination is paralleled by an increase in TSPO radioligand (18F)-GE180 uptake. Comparably, increased uptake of different TSPO ligands, namely, [^{3}H]-(R)-PK11195 [58,68], (123I)-CLINDE [41], and (125I)iodo-DPA-713 [56], has been shown in the cuprizone model. It was suggested that, in the cuprizone model, the observed increase in [3H]-R-PK11195 binding is a result of an increase in the apparent number of binding sites rather than a change in receptor binding affinity [58]. In line with this assumption, we found higher TSPO expression on the protein (Figure 3) and mRNA (Figure 4) level.

The cellular source of TSPO expression in the cuprizone model is not entirely clear. Mattner and colleagues concluded, based on immunflourescence double-labelling experiments, that one of the main sources of TSPO expression in the demyelinated corpus callosum is activated astrocytes. In these studies, virtually all the GFAP-positive astrocytes as well expressed TSPO [41]. Chen and colleagues performed GFAP or Mac-1 immunohistochemistry combined with (3H)-(R)-PK11195 autoradiography and found co-localization of (3H)-(R)-PK11195 binding with both GFAP-expressing astrocytes and Mac-1-expressing microglia [58]. In the current study, we quantified microglia (anti-IBA1) and astrocyte (anti-GFAP) densities and determined the percentage of these cells expressing TSPO. As shown in Figures 5 and 6, most of the IBA1$^+$ cells co-expressed TSPO, whereas just about 30% of the GFAP$^+$ cells co-expressed TSPO. Of note, the mapping of cellular expression of proteins in tissue subjected to cuprizone-induced demyelination is not straightforward. After a 5-week cuprizone intoxication protocol, the midline of the corpus callosum is hypercellular, making it difficult to delineate the border of single cells. Furthermore, GFAP is not always expressed within the entire astrocyte cell body but frequently spares one part of its perinuclear compartment. This anti-GFAP staining pattern causes problems in delineating the exact border of a single astrocyte and, therefore, does not always allow to decide whether a certain protein is expressed within an astrocyte or not. Additionally, the staining efficacy of different antibodies or staining protocols might result in more or less co-localization signals. To further verify that astrocytes express TSPO in the cuprizone model, we processed brain sections of hGFAP-eGFP-mice for anti-TSPO immunoflourescence staining. These mice express eGFP not only in the cell body and proximal processes, but also in the fine distal processes of astrocytes [46]. Furthermore, these mice express eGFP not in all but just a minority of astrocytes. This makes the delineation of single astrocytes easy even in regions with high astrocyte density. As demonstrated in Figure 6C, TSPO expression clearly co-localized to the eGFP signal. In summary, our data provide unequivocal evidence that both activated astrocytes and microglia were responsible for the enhanced [18F]-GE180 binding to TSPO in brain areas undergoing demyelination. Moreover, the bulk of TSPO reactivity in the cuprizone model can be attributed to microglia. Notably, histological and imaging findings in different types of MS lesions indicate that activated microglia are inflammatory modulators, including inactive chronic and cortical lesions, as well as in normal appearing white and grey matter areas [7]. Consequently, imaging microglial activation by PET using radiolabeled TSPO ligands should provide a sensitive marker for neuroinflammatory processes.

High TSPO expression has been demonstrated in various macrophage populations such as in synovial macrophages [69], myocardial macrophages [70], or macrophages of atherosclerotic

plaques [71]. To determine whether recruited monocytes, in addition to microglia, express TSPO, we combined the toxin-induced demyelination model cuprizone with the autoimmune EAE model (i.e., Cup/EAE). As recently demonstrated by our group, cuprizone-induced oligodendrocyte degeneration triggers peripheral immune cell recruitment into the forebrain [43,44]. Here, we utilized transgenic (CX$_3$CR1$^{+/eGFP}$/CCR2$^{+/RFP}$) mice with eGFP-expressing microglia and RFP-expressing monocyte-derived macrophages [47] to investigate which cell type expresses TSPO. As shown in Figure 8J,K, the TSPO signal clearly co-localized to both, eGFP-expressing microglia and RFP-expressing monocyte-derived macrophages. Although not shown in this study, it has been reported that TSPO is as well expressed by CD4$^+$ lymphocytes in EAE [72], as it is in humans [73] and in a model of rheumatoid arthritis [69]. Further studies have to demonstrate to what extent lymphocytes and other peripheral immune cells contribute to the increased TSPO ligand uptake observed in MS lesions.

Axonal degeneration is believed to be a major cause of permanent neurological disability in MS patients. It is assumed that myelinated axons contain two populations of mitochondria: stationary and motile mitochondria. It has been shown that the volume of mitochondrial stationary sites is increased in demyelinated CNS axons [53]. In light of these findings, it is of interest to speculate whether some of the white matter TSPO radioligand uptake observed in PET studies is due to mitochondrial binding in acutely injured axons. 3D reconstructions of serial block-face scanning electron microscopy images showed an accumulation of mitochondria within axonal swellings. Furthermore, immunofluorescence double-labelling experiments revealed accumulations of the mitochondrial protein COXIV at sites of amyloid precursor protein (APP) accumulation (see Figure 7). The most commonly-used marker to visualize axonal transport deficits is the APP [74]. APP is an integral glycoprotein type 1, which is transported towards the axon terminal via anterograde axonal transport [75]. In case of a disturbed axonal transport machinery, APP accumulates at the side of axon injury and can then be visualized by immunohistochemistry as so called "spheroids" [76,77]. Although we found a clear co-localization of COXIV and APP, such a co-localization was not found for TSPO and APP. As already stated above, there is growing realization that axonal degeneration plays a pivotal role in the development of neurological disability in patients with MS. In histopathological studies, acute axonal injury, as defined by the accumulation of APP, was found to occur not only in active demyelinating but also in remyelinating and inactive demyelinated MS lesions [78,79]. Although it is currently not clear why mitochondria do not express TSPO within injured axons, diffuse axonal degeneration probably does not contribute to TSPO-ligand uptake in MS tissues.

PET ligands targeting TSPO represent promising tools to visualize neuroinflammation in MS patients. This may provide information beyond contrast-enhanced MRI and is readily applicable to all patients. This study illustrates that the pathological substrate of an increase in TSPO ligand binding might be diverse including microglia activation, peripheral monocyte recruitment, and astrocytosis.

References

1. Kipp, M.; Nyamoya, S.; Hochstrasser, T.; Amor, S. Multiple sclerosis animal models: A clinical and histopathological perspective. *Brain Pathol.* **2017**, *27*, 123–137. [CrossRef] [PubMed]

2. Kipp, M.; van der Valk, P.; Amor, S. Pathology of multiple sclerosis. *CNS Neurol. Disord. Drug Targets* **2012**, *11*, 506–517. [CrossRef] [PubMed]

3. Lucchinetti, C.F.; Popescu, B.F.; Bunyan, R.F.; Moll, N.M.; Roemer, S.F.; Lassmann, H.; Bruck, W.; Parisi, J.E.; Scheithauer, B.W.; Giannini, C.; et al. Inflammatory cortical demyelination in early multiple sclerosis. *N. Engl. J. Med.* **2011**, *365*, 2188–2197. [CrossRef] [PubMed]

4. Pirko, I.; Lucchinetti, C.F.; Sriram, S.; Bakshi, R. Gray matter involvement in multiple sclerosis. *Neurology* **2007**, *68*, 634–642. [CrossRef] [PubMed]

5. Vercellino, M.; Plano, F.; Votta, B.; Mutani, R.; Giordana, M.T.; Cavalla, P. Grey matter pathology in multiple sclerosis. *J. Neuropathol. Exp. Neurol.* **2005**, *64*, 1101–1107. [CrossRef] [PubMed]

6. Kooi, E.J.; Prins, M.; Bajic, N.; Belien, J.A.; Gerritsen, W.H.; van Horssen, J.; Aronica, E.; van Dam, A.M.; Hoozemans, J.J.; Francis, P.T.; et al. Cholinergic imbalance in the multiple sclerosis hippocampus. *Acta Neuropathol.* **2011**, *122*, 313–322. [CrossRef] [PubMed]

7. Kutzelnigg, A.; Lucchinetti, C.F.; Stadelmann, C.; Bruck, W.; Rauschka, H.; Bergmann, M.; Schmidbauer, M.; Parisi, J.E.; Lassmann, H. Cortical demyelination and diffuse white matter injury in multiple sclerosis. *Brain* **2005**, *128*, 2705–2712. [CrossRef]

8. Hasan, K.M.; Halphen, C.; Kamali, A.; Nelson, F.M.; Wolinsky, J.S.; Narayana, P.A. Caudate nuclei volume, diffusion tensor metrics, and T(2) relaxation in healthy adults and relapsing-remitting multiple sclerosis patients: Implications for understanding gray matter degeneration. *J. Magn. Reson. Imaging* **2009**, *29*, 70–77. [CrossRef]

9. Ontaneda, D.; Thompson, A.J.; Fox, R.J.; Cohen, J.A. Progressive multiple sclerosis: Prospects for disease therapy, repair, and restoration of function. *Lancet* **2017**, *389*, 1357–1366. [CrossRef]

10. Liu, J.; Tian, D.; Murugan, M.; Eyo, U.B.; Dreyfus, C.F.; Wang, W.; Wu, L.J. Microglial Hv1 proton channel promotes cuprizone-induced demyelination through oxidative damage. *J. Neurochem.* **2015**, *135*, 347–356. [CrossRef]

11. Xiao, Y.; Jin, J.; Chang, M.; Chang, J.H.; Hu, H.; Zhou, X.; Brittain, G.C.; Stansberg, C.; Torkildsen, O.; Wang, X.; et al. Peli1 promotes microglia-mediated CNS inflammation by regulating Traf3 degradation. *Nat. Med.* **2013**, *19*, 595–602. [CrossRef] [PubMed]

12. Bauer, J.; Sminia, T.; Wouterlood, F.G.; Dijkstra, C.D. Phagocytic activity of macrophages and microglial cells during the course of acute and chronic relapsing experimental autoimmune encephalomyelitis. *J. Neurosci. Res.* **1994**, *38*, 365–375. [CrossRef] [PubMed]

13. Wlodarczyk, A.; Lobner, M.; Cedile, O.; Owens, T. Comparison of microglia and infiltrating CD11c(+) cells as antigen presenting cells for T cell proliferation and cytokine response. *J. Neuroinflamm.* **2014**, *11*, 57. [CrossRef] [PubMed]

14. Aloisi, F.; Ria, F.; Adorini, L. Regulation of T-cell responses by CNS antigen-presenting cells: Different roles for microglia and astrocytes. *Immunol. Today* **2000**, *21*, 141–147. [CrossRef]

15. Frischer, J.M.; Bramow, S.; Dal-Bianco, A.; Lucchinetti, C.F.; Rauschka, H.; Schmidbauer, M.; Laursen, H.; Sorensen, P.S.; Lassmann, H. The relation between inflammation and neurodegeneration in multiple sclerosis brains. *Brain J. Neurol.* **2009**, *132*, 1175–1189. [CrossRef] [PubMed]

16. Hoflich, K.M.; Beyer, C.; Clarner, T.; Schmitz, C.; Nyamoya, S.; Kipp, M.; Hochstrasser, T. Acute axonal damage in three different murine models of multiple sclerosis: A comparative approach. *Brain Res.* **2016**, *1650*, 125–133. [CrossRef] [PubMed]

17. Minghetti, L.; Levi, G. Microglia as effector cells in brain damage and repair: Focus on prostanoids and nitric oxide. *Prog. Neurobiol.* **1998**, *54*, 99–125. [CrossRef]

18. Ransohoff, R.M.; Perry, V.H. Microglial physiology: Unique stimuli, specialized responses. *Annu. Rev. Immunol.* **2009**, *27*, 119–145. [CrossRef]

19. Venneti, S.; Lopresti, B.J.; Wiley, C.A. The peripheral benzodiazepine receptor (Translocator protein 18kDa) in microglia: From pathology to imaging. *Prog. Neurobiol.* **2006**, *80*, 308–322. [CrossRef]

20. McEnery, M.W.; Snowman, A.M.; Trifiletti, R.R.; Snyder, S.H. Isolation of the mitochondrial benzodiazepine receptor: Association with the voltage-dependent anion channel and the adenine nucleotide carrier. *Proc. Natl. Acad. Sci. USA* **1992**, *89*, 3170–3174. [CrossRef]

21. Yeliseev, A.A.; Kaplan, S. A sensory transducer homologous to the mammalian peripheral-type benzodiazepine receptor regulates photosynthetic membrane complex formation in Rhodobacter sphaeroides 2.4.1. *J. Biol. Chem.* **1995**, *270*, 21167–21175. [CrossRef] [PubMed]

22. Papadopoulos, V.; Berkovich, A.; Krueger, K.E.; Costa, E.; Guidotti, A. Diazepam binding inhibitor and its processing products stimulate mitochondrial steroid biosynthesis via an interaction with mitochondrial benzodiazepine receptors. *Endocrinology* **1991**, *129*, 1481–1488. [CrossRef] [PubMed]

23. Denora, N.; Natile, G. An Updated View of Translocator Protein (TSPO). *Int. J. Mol. Sci.* **2017**, 18. [CrossRef] [PubMed]

24. McNeela, A.M.; Bernick, C.; Hines, R.M.; Hines, D.J. TSPO regulation in reactive gliotic diseases. *J. Neurosci. Res.* **2018**, *96*, 978–988. [CrossRef] [PubMed]

25. Cosenza-Nashat, M.; Zhao, M.L.; Suh, H.S.; Morgan, J.; Natividad, R.; Morgello, S.; Lee, S.C. Expression of the translocator protein of 18 kDa by microglia, macrophages and astrocytes based on immunohistochemical localization in abnormal human brain. *Neuropathol. Appl. Neurobiol.* **2009**, *35*, 306–328. [CrossRef] [PubMed]

26. Maeda, J.; Higuchi, M.; Inaji, M.; Ji, B.; Haneda, E.; Okauchi, T.; Zhang, M.R.; Suzuki, K.; Suhara, T. Phase-dependent roles of reactive microglia and astrocytes in nervous system injury as delineated by imaging of peripheral benzodiazepine receptor. *Brain Res.* **2007**, *1157*, 100–111. [CrossRef] [PubMed]

27. Takaya, S.; Hashikawa, K.; Turkheimer, F.E.; Mottram, N.; Deprez, M.; Ishizu, K.; Kawashima, H.; Akiyama, H.; Fukuyama, H.; Banati, R.B.; et al. The lack of expression of the peripheral benzodiazepine receptor characterises microglial response in anaplastic astrocytomas. *J. Neuro-Oncol.* **2007**, *85*, 95–103. [CrossRef]

28. Kuhlmann, A.C.; Guilarte, T.R. Cellular and subcellular localization of peripheral benzodiazepine receptors after trimethyltin neurotoxicity. *J. Neurochem.* **2000**, *74*, 1694–1704. [CrossRef]

29. Banati, R.B. Visualising microglial activation in vivo. *Glia* **2002**, *40*, 206–217. [CrossRef]

30. Zivadinov, R.; Stosic, M.; Cox, J.L.; Ramasamy, D.P.; Dwyer, M.G. The place of conventional MRI and newly emerging MRI techniques in monitoring different aspects of treatment outcome. *J. Neurol.* **2008**, *255*, 61–74. [CrossRef]

31. Hagens, M.; van Berckel, B.; Barkhof, F. Novel MRI and PET markers of neuroinflammation in multiple sclerosis. *Curr. Opin. Neurol.* **2016**, *29*, 229–236. [CrossRef] [PubMed]

32. Vowinckel, E.; Reutens, D.; Becher, B.; Verge, G.; Evans, A.; Owens, T.; Antel, J.P. PK11195 binding to the peripheral benzodiazepine receptor as a marker of microglia activation in multiple sclerosis and experimental autoimmune encephalomyelitis. *J. Neurosci. Res.* **1997**, *50*, 345–353. [CrossRef]

33. Wickstrom, T.; Clarke, A.; Gausemel, I.; Horn, E.; Jorgensen, K.; Khan, I.; Mantzilas, D.; Rajanayagam, T.; In't Veld, D.J.; Trigg, W. The development of an automated and GMP compliant FASTlab Synthesis of [(18) F]GE-180; a radiotracer for imaging translocator protein (TSPO). *J. Label. Compd. Radiopharm.* **2014**, *57*, 42–48. [CrossRef] [PubMed]

34. Unterrainer, M.; Mahler, C.; Vomacka, L.; Lindner, S.; Havla, J.; Brendel, M.; Boning, G.; Ertl-Wagner, B.; Kumpfel, T.; Milenkovic, V.M.; et al. TSPO PET with [(18)F]GE-180 sensitively detects focal neuroinflammation in patients with relapsing-remitting multiple sclerosis. *Eur. J. Nucl. Med. Mol. Imaging* **2018**, *45*, 1423–1431. [CrossRef] [PubMed]

35. Vomacka, L.; Albert, N.L.; Lindner, S.; Unterrainer, M.; Mahler, C.; Brendel, M.; Ermoschkin, L.; Gosewisch, A.; Brunegraf, A.; Buckley, C.; et al. TSPO imaging using the novel PET ligand [(18)F]GE-180: Quantification approaches in patients with multiple sclerosis. *EJNMMI Res.* **2017**, *7*, 89. [CrossRef] [PubMed]

36. Blume, T.; Focke, C.; Peters, F.; Deussing, M.; Albert, N.L.; Lindner, S.; Gildehaus, F.J.; von Ungern-Sternberg, B.; Ozmen, L.; Baumann, K.; et al. Microglial response to increasing amyloid load saturates with aging: A longitudinal dual tracer in vivo muPET-study. *J. Neuroinflamm.* **2018**, *15*, 307. [CrossRef] [PubMed]

37. Klein, B.; Mrowetz, H.; Barker, C.M.; Lange, S.; Rivera, F.J.; Aigner, L. Age Influences Microglial Activation After Cuprizone-Induced Demyelination. *Front. Aging Neurosci.* **2018**, *10*, 278. [CrossRef] [PubMed]

38. Airas, L.; Dickens, A.M.; Elo, P.; Marjamaki, P.; Johansson, J.; Eskola, O.; Jones, P.A.; Trigg, W.; Solin, O.; Haaparanta-Solin, M.; et al. In vivo PET imaging demonstrates diminished microglial activation after fingolimod treatment in an animal model of multiple sclerosis. *J. Nucl. Med.* **2015**, *56*, 305–310. [CrossRef]

39. Mattner, F.; Staykova, M.; Berghofer, P.; Wong, H.J.; Fordham, S.; Callaghan, P.; Jackson, T.; Pham, T.; Gregoire, M.C.; Zahra, D.; et al. Central nervous system expression and PET imaging of the translocator protein in relapsing-remitting experimental autoimmune encephalomyelitis. *J. Nucl. Med.* **2013**, *54*, 291–298. [CrossRef]

40. Abourbeh, G.; Theze, B.; Maroy, R.; Dubois, A.; Brulon, V.; Fontyn, Y.; Dolle, F.; Tavitian, B.; Boisgard, R. Imaging microglial/macrophage activation in spinal cords of experimental autoimmune encephalomyelitis rats by positron emission tomography using the mitochondrial 18 kDa translocator protein radioligand [(1)(8)F]DPA-714. *J. Neurosci.* **2012**, *32*, 5728–5736. [CrossRef]

41. Mattner, F.; Bandin, D.L.; Staykova, M.; Berghofer, P.; Gregoire, M.C.; Ballantyne, P.; Quinlivan, M.; Fordham, S.; Pham, T.; Willenborg, D.O.; et al. Evaluation of [(1)(2)(3)I]-CLINDE as a potent SPECT radiotracer to assess the degree of astroglia activation in cuprizone-induced neuroinflammation. *Eur. J. Nucl. Med. Mol. Imaging* **2011**, *38*, 1516–1528. [CrossRef] [PubMed]

42. Notter, T.; Coughlin, J.M.; Gschwind, T.; Weber-Stadlbauer, U.; Wang, Y.; Kassiou, M.; Vernon, A.C.; Benke, D.; Pomper, M.G.; Sawa, A.; et al. Translational evaluation of translocator protein as a marker of neuroinflammation in schizophrenia. *Mol. Psychiatry* **2018**, *23*, 323–334. [CrossRef] [PubMed]

43. Ruther, B.J.; Scheld, M.; Dreymueller, D.; Clarner, T.; Kress, E.; Brandenburg, L.O.; Swartenbroekx, T.; Hoornaert, C.; Ponsaerts, P.; Fallier-Becker, P.; et al. Combination of cuprizone and experimental autoimmune encephalomyelitis to study inflammatory brain lesion formation and progression. *Glia* **2017**, *65*, 1900–1913. [CrossRef]

44. Scheld, M.; Ruther, B.J.; Grosse-Veldmann, R.; Ohl, K.; Tenbrock, K.; Dreymuller, D.; Fallier-Becker, P.; Zendedel, A.; Beyer, C.; Clarner, T.; et al. Neurodegeneration Triggers Peripheral Immune Cell Recruitment into the Forebrain. *J. Neurosci.* **2016**, *36*, 1410–1415. [CrossRef] [PubMed]

45. Nyamoya, S.; Leopold, P.; Becker, B.; Beyer, C.; Hustadt, F.; Schmitz, C.; Michel, A.; Kipp, M. G-Protein-Coupled Receptor Gpr17 Expression in Two Multiple Sclerosis Remyelination Models. *Mol. Neurobiol.* **2018**. [CrossRef] [PubMed]

46. Nolte, C.; Matyash, M.; Pivneva, T.; Schipke, C.G.; Ohlemeyer, C.; Hanisch, U.K.; Kirchhoff, F.; Kettenmann, H. GFAP promoter-controlled EGFP-expressing transgenic mice: A tool to visualize astrocytes and astrogliosis in living brain tissue. *Glia* **2001**, *33*, 72–86. [CrossRef]

47. Saederup, N.; Cardona, A.E.; Croft, K.; Mizutani, M.; Cotleur, A.C.; Tsou, C.L.; Ransohoff, R.M.; Charo, I.F. Selective chemokine receptor usage by central nervous system myeloid cells in CCR2-red fluorescent protein knock-in mice. *PLoS ONE* **2010**, *5*, e13693. [CrossRef]

48. Brendel, M.; Probst, F.; Jaworska, A.; Overhoff, F.; Korzhova, V.; Albert, N.L.; Beck, R.; Lindner, S.; Gildehaus, F.J.; Baumann, K.; et al. Glial Activation and Glucose Metabolism in a Transgenic Amyloid Mouse Model: A Triple-Tracer PET Study. *J. Nucl. Med.* **2016**, *57*, 954–960. [CrossRef]

49. Overhoff, F.; Brendel, M.; Jaworska, A.; Korzhova, V.; Delker, A.; Probst, F.; Focke, C.; Gildehaus, F.J.; Carlsen, J.; Baumann, K.; et al. Automated Spatial Brain Normalization and Hindbrain White Matter Reference Tissue Give Improved [(18)F]-Florbetaben PET Quantitation in Alzheimer's Model Mice. *Front. Neurosci.* **2016**, *10*, 45. [CrossRef]

50. Deussing, M.; Blume, T.; Vomacka, L.; Mahler, C.; Focke, C.; Todica, A.; Unterrainer, M.; Albert, N.L.; Lindner, S.; von Ungern-Sternberg, B.; et al. Coupling between physiological TSPO expression in brain and myocardium allows stabilization of late-phase cerebral [(18)F]GE180 PET quantification. *NeuroImage* **2017**, *165*, 83–91. [CrossRef]

51. Slowik, A.; Schmidt, T.; Beyer, C.; Amor, S.; Clarner, T.; Kipp, M. The sphingosine 1-phosphate receptor agonist FTY720 is neuroprotective after cuprizone-induced CNS demyelination. *Br. J. Pharmacol.* **2015**, *172*, 80–92. [CrossRef] [PubMed]

52. Baertling, F.; Kokozidou, M.; Pufe, T.; Clarner, T.; Windoffer, R.; Wruck, C.J.; Brandenburg, L.O.; Beyer, C.; Kipp, M. ADAM12 is expressed by astrocytes during experimental demyelination. *Brain Res.* **2010**, *1326*, 1–14. [CrossRef] [PubMed]

53. Ohno, N.; Chiang, H.; Mahad, D.J.; Kidd, G.J.; Liu, L.; Ransohoff, R.M.; Sheng, Z.H.; Komuro, H.; Trapp, B.D. Mitochondrial immobilization mediated by syntaphilin facilitates survival of demyelinated axons. *Proc. Natl. Acad. Sci. USA* **2014**, *111*, 9953–9958. [CrossRef] [PubMed]

54. Kipp, M.; Clarner, T.; Dang, J.; Copray, S.; Beyer, C. The cuprizone animal model: New insights into an old story. *Acta Neuropathol.* **2009**, *118*, 723–736. [CrossRef] [PubMed]

55. Fan, Z.; Calsolaro, V.; Atkinson, R.A.; Femminella, G.D.; Waldman, A.; Buckley, C.; Trigg, W.; Brooks, D.J.; Hinz, R.; Edison, P. Flutriciclamide (18F-GE180) PET: First-in-Human PET Study of Novel Third-Generation In Vivo Marker of Human Translocator Protein. *J. Nucl. Med.* **2016**, *57*, 1753–1759. [CrossRef] [PubMed]

56. Fukudome, D.; Hayes, L.N.; Faust, T.E.; Foss, C.A.; Kondo, M.A.; Lee, B.J.; Saito, A.; Kano, S.I.; Coughlin, J.M.; Kamiya, A.; et al. Translocator protein (TSPO) and stress cascades in mouse models of psychosis with inflammatory disturbances. *Schizophr. Res.* **2018**. [CrossRef] [PubMed]

57. Vlodavsky, E.; Soustiel, J.F. Immunohistochemical expression of peripheral benzodiazepine receptors in human astrocytomas and its correlation with grade of malignancy, proliferation, apoptosis and survival. *J. Neurooncol.* **2007**, *81*, 1–7. [CrossRef]

58. Chen, M.K.; Baidoo, K.; Verina, T.; Guilarte, T.R. Peripheral benzodiazepine receptor imaging in CNS demyelination: Functional implications of anatomical and cellular localization. *Brain* **2004**, *127*, 1379–1392. [CrossRef]

59. Clarner, T.; Diederichs, F.; Berger, K.; Denecke, B.; Gan, L.; van der Valk, P.; Beyer, C.; Amor, S.; Kipp, M. Myelin debris regulates inflammatory responses in an experimental demyelination animal model and multiple sclerosis lesions. *Glia* **2012**, *60*, 1468–1480. [CrossRef]

60. Mahad, D.J.; Ziabreva, I.; Campbell, G.; Lax, N.; White, K.; Hanson, P.S.; Lassmann, H.; Turnbull, D.M. Mitochondrial changes within axons in multiple sclerosis. *Brain* **2009**, *132*, 1161–1174. [CrossRef]

61. Zambonin, J.L.; Zhao, C.; Ohno, N.; Campbell, G.R.; Engeham, S.; Ziabreva, I.; Schwarz, N.; Lee, S.E.; Frischer, J.M.; Turnbull, D.M.; et al. Increased mitochondrial content in remyelinated axons: Implications for multiple sclerosis. *Brain* **2011**, *134*, 1901–1913. [CrossRef] [PubMed]

62. Hiremath, M.M.; Chen, V.S.; Suzuki, K.; Ting, J.P.; Matsushima, G.K. MHC class II exacerbates demyelination in vivo independently of T cells. *J. Neuroimmunol.* **2008**, *203*, 23–32. [CrossRef] [PubMed]

63. Banati, R.B.; Goerres, G.W.; Myers, R.; Gunn, R.N.; Turkheimer, F.E.; Kreutzberg, G.W.; Brooks, D.J.; Jones, T.; Duncan, J.S. [11C](R)-PK11195 positron emission tomography imaging of activated microglia in vivo in Rasmussen's encephalitis. *Neurology* **1999**, *53*, 2199–2203. [CrossRef]

64. Junck, L.; Olson, J.M.; Ciliax, B.J.; Koeppe, R.A.; Watkins, G.L.; Jewett, D.M.; McKeever, P.E.; Wieland, D.M.; Kilbourn, M.R.; Starosta-Rubinstein, S.; et al. PET imaging of human gliomas with ligands for the peripheral benzodiazepine binding site. *Ann. Neurol.* **1989**, *26*, 752–758. [CrossRef] [PubMed]

65. Banati, R.B. Neuropathological imaging: In vivo detection of glial activation as a measure of disease and adaptive change in the brain. *Br. Med. Bull.* **2003**, *65*, 121–131. [CrossRef] [PubMed]

66. Banati, R.B.; Newcombe, J.; Gunn, R.N.; Cagnin, A.; Turkheimer, F.; Heppner, F.; Price, G.; Wegner, F.; Giovannoni, G.; Miller, D.H.; et al. The peripheral benzodiazepine binding site in the brain in multiple sclerosis: Quantitative in vivo imaging of microglia as a measure of disease activity. *Brain J. Neurol.* **2000**, *123*, 2321–2337. [CrossRef]

67. Kreisl, W.C.; Fujita, M.; Fujimura, Y.; Kimura, N.; Jenko, K.J.; Kannan, P.; Hong, J.; Morse, C.L.; Zoghbi, S.S.; Gladding, R.L.; et al. Comparison of [(11)C]-(R)-PK 11195 and [(11)C]PBR28, two radioligands for translocator protein (18 kDa) in human and monkey: Implications for positron emission tomographic imaging of this inflammation biomarker. *NeuroImage* **2010**, *49*, 2924–2932. [CrossRef] [PubMed]

68. Chen, M.K.; Guilarte, T.R. Imaging the peripheral benzodiazepine receptor response in central nervous system demyelination and remyelination. *Toxicol. Sci.* **2006**, *91*, 532–539. [CrossRef]

69. Narayan, N.; Owen, D.; Mandhair, H.; Smyth, E.; Carlucci, F.; Saleem, A.; Gunn, R.; Rabiner, E.I.A.; Wells, L.; Dakin, S.; et al. Translocator Protein as an Imaging Marker of Macrophage and Stromal Activation in RA Pannus. *J. Nucl. Med.* **2018**, *59*, 1125–1132. [CrossRef]

70. Thackeray, J.T.; Hupe, H.C.; Wang, Y.; Bankstahl, J.P.; Berding, G.; Ross, T.L.; Bauersachs, J.; Wollert, K.C.; Bengel, F.M. Myocardial Inflammation Predicts Remodeling and Neuroinflammation After Myocardial Infarction. *J. Am. Coll. Cardiol.* **2018**, *71*, 263–275. [CrossRef]

71. Hellberg, S.; Silvola, J.M.U.; Kiugel, M.; Liljenback, H.; Savisto, N.; Li, X.G.; Thiele, A.; Lehmann, L.; Heinrich, T.; Vollmer, S.; et al. 18-kDa translocator protein ligand (18)F-FEMPA: Biodistribution and uptake into atherosclerotic plaques in mice. *J. Nucl. Cardiol.* **2017**, *24*, 862–871. [CrossRef] [PubMed]

72. Fernandez Hurst, N.; Zanetti, S.R.; Baez, N.S.; Bibolini, M.J.; Bouzat, C.; Roth, G.A. Diazepam treatment reduces inflammatory cells and mediators in the central nervous system of rats with experimental autoimmune encephalomyelitis. *J. Neuroimmunol.* **2017**, *313*, 145–151. [CrossRef] [PubMed]

73. Berkovich, A.; Ferrarese, C.; Cavaletti, G.; Alho, H.; Marzorati, C.; Bianchi, G.; Guidotti, A.; Costa, E. Topology of two DBI receptors in human lymphocytes. *Life Sci.* **1993**, *52*, 1265–1277. [CrossRef]

74. Matsushima, G.K.; Morell, P. The neurotoxicant, cuprizone, as a model to study demyelination and remyelination in the central nervous system. *Brain Pathol.* **2001**, *11*, 107–116. [CrossRef] [PubMed]

75. Koo, E.H.; Sisodia, S.S.; Archer, D.R.; Martin, L.J.; Weidemann, A.; Beyreuther, K.; Fischer, P.; Masters, C.L.; Price, D.L. Precursor of amyloid protein in Alzheimer disease undergoes fast anterograde axonal transport. *Proc. Natl. Acad. Sci. USA* **1990**, *87*, 1561–1565. [CrossRef] [PubMed]

76. Sherriff, F.E.; Bridges, L.R.; Gentleman, S.M.; Sivaloganathan, S.; Wilson, S. Markers of axonal injury in post mortem human brain. *Acta Neuropathol.* **1994**, *88*, 433–439. [CrossRef] [PubMed]

77. Stone, J.R.; Singleton, R.H.; Povlishock, J.T. Antibodies to the C-terminus of the beta-amyloid precursor protein (APP): A site specific marker for the detection of traumatic axonal injury. *Brain Res.* **2000**, *871*, 288–302. [CrossRef]

78. Bitsch, A.; Schuchardt, J.; Bunkowski, S.; Kuhlmann, T.; Bruck, W. Acute axonal injury in multiple sclerosis. Correlation with demyelination and inflammation. *Brain* **2000**, *123*, 1174–1183. [CrossRef]

79. Khademi, M.; Dring, A.M.; Gilthorpe, J.D.; Wuolikainen, A.; Al Nimer, F.; Harris, R.A.; Andersson, M.; Brundin, L.; Piehl, F.; Olsson, T.; et al. Intense inflammation and nerve damage in early multiple sclerosis subsides at older age: A reflection by cerebrospinal fluid biomarkers. *PLoS ONE* **2013**, *8*, e63172. [CrossRef]

8.2 Evaluation strategy to determine reliable demyelination in the cuprizone model

SHORT COMMUNICATION

CrossMark

Evaluation strategy to determine reliable demyelination in the cuprizone model

Uta Chrzanowski[1] · Christoph Schmitz[1] · Anja Horn-Bochtler[2] · Anne Nack[1] · Markus Kipp[1,3]

Abstract

In multiple sclerosis patients, chronic clinical deficits are known to result from axonal degeneration which is triggered by inadequate remyelination. The underlying molecular mechanisms of remyelination and its failure remain currently unclear. In vivo models, among the cuprizone model, are valuable tools to study underlying mechanisms of remyelination and its failure. Since complete and reproducible demyelination of the analyzed brain region is an indispensable prerequisite for efficient remyelination experiments, in this study we systematically addressed which part of the corpus callosum is reliably and consistently demyelinated after acute cuprizone-induced demyelination. Following a novel evaluation strategy, we can show that at the level of the rostral hippocampus, the most medial sectors of the corpus callosum (spanning 500 μm in the horizontal plane) are consistently demyelinated, whereas more lateral sectors show inconsistent and incomplete demyelination. These results precisely define a part of the corpus callosum which should be used as a region of interest during remyelination experiments.

Keywords Cuprizone · Demyelination · Remyelination · Optical density · Regeneration

Introduction

Remyelination, which follows the pathological loss of myelin in diseases like Multiple sclerosis (MS), is a reparative process believed to ameliorate neurodegeneration. While remyelination occurs in many MS lesions (Prineas et al. 1993), it can become increasingly incomplete/inadequate or eventually it completely fails (Patrikios et al. 2006). Understanding why a relatively robust regenerative process should lose momentum is an important prerequisite for developing an effective therapeutic approach. One frequently applied preclinical model to study the effectiveness of drugs to boost remyelination is the cuprizone model (Slowik et al. 2015). The extent of de- and remyelination in this model is frequently determined by the semi-quantification of myelin protein expression via optical density measurements (Slowik et al. 2015; Werneburg et al. 2017). Commonly visualized myelin proteins are proteolipid protein (PLP), myelin associated glycoprotein (MAG), myelin basic protein (MBP) or 2',3'-cyclic-nucleotide 3'-phosphodiesterase (CNPase), and the analyzed region of interest is the midline of the corpus callosum at the level of the rostral hippocampus (*see* Fig. 1a). However, as recently demonstrated by our and other groups, demyelination is not spread evenly across the corpus callosum (Schmidt et al. 2013). Since consistent and reproducible demyelination is an indispensable prerequisite for efficient remyelination studies, the aim of this study was to analyze which part of the midline of the corpus callosum is consistently demyelinated and, therefore, should be used as a region of interest (ROI) in remyelination studies.

✉ Markus Kipp
markus.kipp@med.uni-rostock.de

1 Department of Anatomy II, Ludwig-Maximilians-University of Munich, 80336 Munich, Germany

2 Department of Anatomy I, Ludwig-Maximilians-University of Munich, 80336 Munich, Germany

3 Institute of Anatomy, Rostock University Medical Center, Gertrudenstrasse 9, 18056 Rostock, Germany

Methods

Animals and cuprizone-induced demyelination

6–7 week-old C57BL/6 male mice (19 g - 20 g) were purchased from Janvier Labs (Le Genest-Saint-Isle, France). Microbiological monitoring was performed according to the Federation of European Laboratory Animal Science
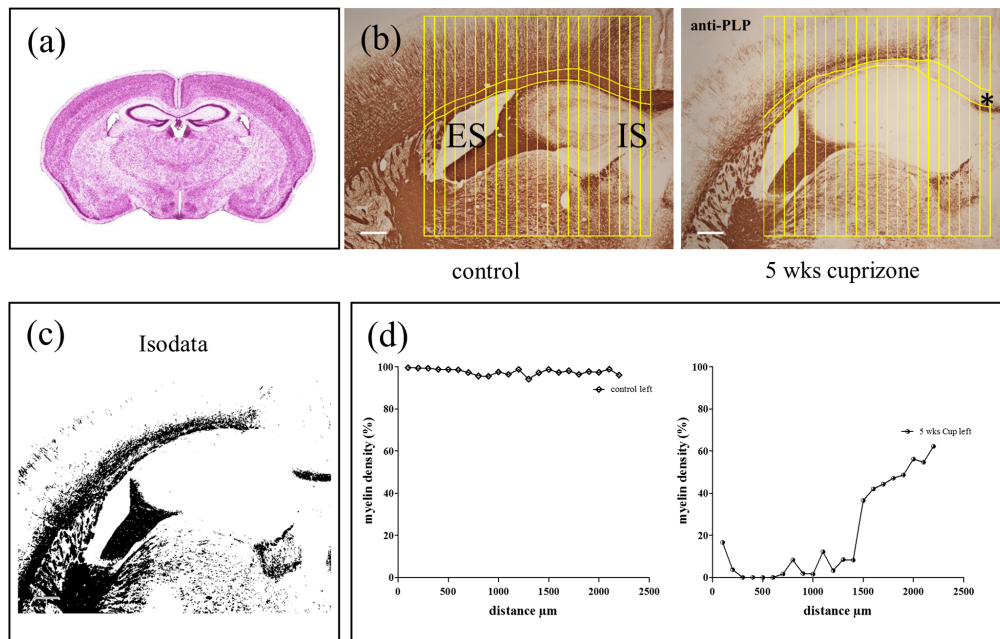
🍂 Springer

46

Fig. 1 **a** Brain level at which immunohistochemistry was performed. **b** Representative anti-PLP (proteolipid protein) stained section of a control and 5 weeks (wks) cuprizone (Cup)-intoxicated mouse. Corpus callosum sectors are outlined by the yellow columns. The star indicates the most internal corpus callosum sector. ES (external sector); IS (internal sector). **c** Representative illustration of a binary picture after thresholding using the *Isodata* algorithm provided by the ImageJ software package. **d** Representative result of staining intensity within the different corpus callosum sectors. 100 means a fully myelinated, zero a completely demyelinated corpus callosum sector. Each sector spans over a horizontal distance of 100 μm. Scale bars: (b/c) 250 μm

Associations recommendations. Experiments have been approved by the Regierung Oberbayern (reference number 55.2-154-2532-73-15) and conducted following guidelines of the Federation of European Laboratory Animal Science Associations (FELASA). Cuprizone-intoxication (0.25%) was performed as described previously for 1, 3 or 5 weeks (Hochstrasser et al. 2017). At the end of the experiment, mice were deeply anaesthetized with ketamine (100 mg·kg − 1 i.p.) and xylazine (10 mg·kg − 1 i.p.) and transcardially perfused with ice-cold PBS followed by a 3.7% paraformaldehyde solution (PFA; pH 7.4). Brains were subsequently dissected, embedded in paraffin, and then coronal sections (5 μm) were prepared.

Immunohistochemical evaluation

Established protocols were used for immunohistochemistry (Slowik et al. 2015). In brief, sections were rehydrated and, if necessary, antigens were unmasked with Tris/EDTA buffer (pH 9.0) or citrate (pH 6.0) heating. After washing in PBS, sections were incubated overnight (4 °C) with the primary antibodies diluted in blocking solution (serum of species in which the secondary antibody was produced). The following primary antibodies were used: anti-PLP (1:5000, Serotec, MCA839G; Puchheim, Germany), anti-MAG (1:4000, Abcam, ab89780; Cambridge, UK), anti-CNPase (1:2000, Abcam, ab6313; Cambridge, UK), and anti-MBP (1:500, Abcam, ab7349; Cambridge, UK). The next day, slides were incubated with biotinylated secondary antibodies (both 1:200, Vector Labs, Dossenheim, Germany; anti- mouse, BA9200; anti- rat, BA9400) for 1 h and then with peroxidase-coupled avidin-biotin complex (ABC kit; Vector Laboratories, Peterborough, UK) and treated with 3,3'-diaminobenzidine (DAKO, Hamburg, Germany) as a peroxidase substrate.

Fig. 2 **a** Anti-PLP (proteolipid protein), **b** anti-MAG (myelin associated ▶ glycoprotein) and **c** anti-CNPase (2',3'-cyclic-nucleotide 3'-phosphodies-terase) staining intensity in 22 corpus callosum sectors. 100 means a fully myelinated, zero a completely demyelinated corpus callosum sector. Each sector spans over a horizontal distance of 100 μm (blue line: first five sectors = 500 μm). Representative images from control, 1, 3 and 5 wks (weeks) cuprizone (Cup) intoxicated mice are shown on the right. * $p < 0.05$, ** $p < 0.01$ and *** $p < 0.001$; Mann Whitney test. Scale bars: (a-c) 250 μm

(a) PLP

(b) MAG

(c) CNPase
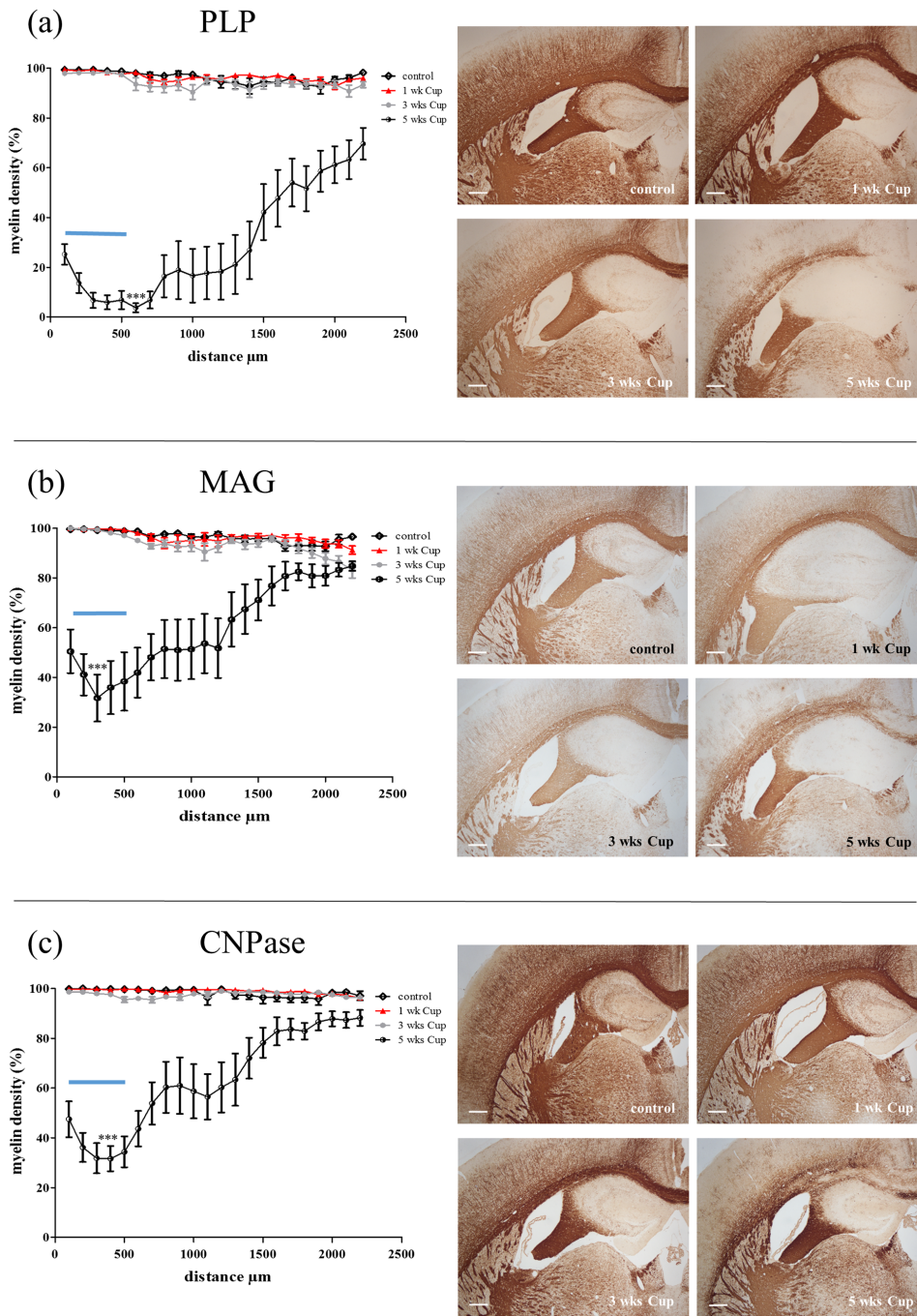
Stained sections were digitalized using a Nikon ECLIPSE E200 microscope (Nikon Instruments, Düsseldorf, Germany) equipped with a DS-2Mv camera.

Stained sections were evaluated by densitometry of the staining intensity using ImageJ and automated thresholding. To evaluate the reproducibility of cuprizone-induced demyelination in different sectors of the midline of the corpus callosum, the following strategy was followed: First, the midline of the corpus callosum was outlined, and then superimposed by a grid (distance between adjacent yellow lines = 100 μm, *see* Fig. 1b). After applying the *Isodata* threshold algorithm to obtain a binary image (*see* Fig. 1c), the optical density was measured in the individual fields, and subsequently blotted against the distance of the midline of the corpus callosum (star in Fig. 1b). Those parts of the corpus callosum near the midline are called "internal sectors" (IS in Fig. 1b) whereas those parts of the corpus callosum near the lateral ventricles are called "external sectors" (ES in Fig. 1b). Right and left hemispheres were separately evaluated, and results were averaged. A representative result of anti-PLP-processed slides from a control and 5 weeks cuprizone-intoxicated mouse is shown in Fig. 1d.

Statistics

Statistical analyses were performed using Prism 5 (GraphPad Software Inc., San Diego, CA, USA). All data are given as arithmetic means ± SEMs. A *p* value of <0.05 was considered to be statistically significant. Applied statistical tests are given in the respective figure legends. No outliers were excluded from the analyses. Kolmogorov-Smirnov test was applied to test for normal distribution of the data. Four control and five cuprizone animals (each time point) were used per experimental group.

Results

As demonstrated in Fig. 2, a homogenous anti-PLP, anti-MAG and anti-CNPase staining intensity was observed in all corpus callosum sectors of control and 1 week (wk) cuprizone-intoxicated mice. While similar results were obtained at week 3 for anti-PLP and anti-CNPase stained sections, a slight yet significant drop of anti-MAG staining intensity was observed in the external sectors of the corpus callosum midline. Statistical comparison using one-way ANOVA with the obtained *p* values corrected for multiple testing using Bonferronni's method revealed a significant loss of anti-MAG staining intensities within the four most external sectors compared to the most internal sector. At week 5, a significant loss of anti-PLP, anti-MAG, and anti-CNPase-staining intensities were evident in the internal sectors of the corpus callosum. The mean loss of myelin protein staining intensity

within the five internal sectors was for PLP ~96% (control = 97.96 ± 0.74 versus 5 wks 3.69 ± 1.80 relative optical density; $p < 0.001$), for MAG ~68% (control = 99.22 ± 0.20 versus 5 wks 31.68 ± 9.46; $p < 0.001$), and for CNPase ~68% (control = 99.73 ± 0.14 versus 5 wks 31.64 ± 5.07; $p < 0.001$). Similar results were obtained for MBP ~62% (control = 98.76 ± 0.27 versus 5 wks 36.96 ± 6.15; $p < 0.001$; data not shown). Of note, the first five sectors, compromising a distance of 500 μm from the midline of the corpus callosum, showed most severe demyelination in all three applied immunohistochemical stains (blue lines in Fig. 2), whereas more lateral orientated sectors showed incomplete demyelination.

Discussion

In this study we addressed the reproducibility of demyelination within different corpus callosum subsectors. Following conventional protocols, acute demyelination is induced by a 5 weeks cuprizone intoxication period, and then pharmaceutical interventions are initiated to test for promyelinating drug effects (Slowik et al. 2015). Reproducible and preferably complete demyelination is an indispensable prerequisite for reliable remyelination studies (Stidworthy et al. 2003). Therefore, it is important to know which parts of the corpus callosum are demyelinated in a reproducible manner at week 5 before remyelination interventions are initiated. In vivo imaging methods are currently developed to visualize the myelination levels of the corpus callosum in living mice (Cao et al. 2018; de Paula Faria et al. 2014). Although such methods could help in the near future to monitor the efficacy of new drugs aimed at restoring myelin, their resolution is currently insufficient to visualize the extent of demyelination in corpus callosum subregions. Here, we show that demyelination is extensive and reproducible within the internal 500 μm spanning corpus callosum segments. Optical densities especially in anti-PLP stained sections show low standard error of the mean values. We, thus, recommend to focus on this callosal subregion during remyelination trials. Of note, this statement is true for the corpus callosum at the level of the rostral hippocampus. More rostral parts of the corpus callosum, such as at the level of the anterior commissure, might have a different demyelination pattern.

The observation that MAG- but not PLP- or CNPase-staining intensity was significantly reduced after 3 weeks of cuprizone intoxication is remarkable, although this finding has to be verified using other anti-myelin antibodies. It has been suggested that cuprizone-induced oligodendrocyte apoptosis mimics the pathology of so called "type-III MS lesions" (Lucchinetti et al. 2000). Such lesions are characterized by a selective reduction of MAG protein, and are reminiscent of virus- or toxin-induced demyelination rather than autoimmunity. Although further studies have to verify this observation,

selective early MAG loss in the cuprizone model further suggests that the mode of cuprizone-induced oligodendrocyte degeneration might well be relevant for MS.

Compliance with ethical standards

Conflict of interest   The authors declare no competing financial interests.

Publisher's note Springer Nature remains neutral with regard to jurisdictional claims in published maps and institutional affiliations.

References

Cao J, Hu Y, Shazeeb MS, Pedraza CE, Pande N, Weinstock D, Polites GH, Zhang W, Chandross KJ, Ying X (2018) In vivo optical imaging of myelination events in a myelin basic protein promoter-driven luciferase transgenic mouse model. ASN Neuro 10: 1759091418777329. https://doi.org/10.1177/1759091418777329

de Paula Faria D, de Vries EF, Sijbesma JW, Dierckx RA, Buchpiguel CA, Copray S (2014) PET imaging of demyelination and remyelination in the cuprizone mouse model for multiple sclerosis: a comparison between [11C]CIC and [11C]MeDAS. Neuroimage 87:395–402. https://doi.org/10.1016/j.neuroimage.2013.10.057

Hochstrasser T, Exner GL, Nyamoya S, Schmitz C, Kipp M (2017) Cuprizone-containing pellets are less potent to induce consistent demyelination in the Corpus Callosum of C57BL/6 mice. J Mol Neurosci: MN 61:617–624. https://doi.org/10.1007/s12031-017-0903-3

Lucchinetti C, Bruck W, Parisi J, Scheithauer B, Rodriguez M, Lassmann H (2000) Heterogeneity of multiple sclerosis lesions: implications for the pathogenesis of demyelination. Ann Neurol 47:707–717

Patrikios P, Stadelmann C, Kutzelnigg A, Rauschka H, Schmidbauer M, Laursen H, Sorensen PS, Bruck W, Lucchinetti C, Lassmann H (2006) Remyelination is extensive in a subset of multiple sclerosis patients. Brain 129:3165–3172. https://doi.org/10.1093/brain/awl217

Prineas JW, Barnard RO, Kwon EE, Sharer LR, Cho ES (1993) Multiple sclerosis: remyelination of nascent lesions. Ann Neurol 33:137–151. https://doi.org/10.1002/ana.410330203

Schmidt T, Awad H, Slowik A, Beyer C, Kipp M, Clarner T (2013) Regional heterogeneity of cuprizone-induced demyelination: topographical aspects of the midline of the corpus callosum. J Mol Neurosci: MN 49:80–88. https://doi.org/10.1007/s12031-012-9896-0

Slowik A, Schmidt T, Beyer C, Amor S, Clarner T, Kipp M (2015) The sphingosine 1-phosphate receptor agonist FTY720 is neuroprotective after cuprizone-induced CNS demyelination. Br J Pharmacol 172:80–92. https://doi.org/10.1111/bph.12938

Stidworthy MF, Genoud S, Suter U, Mantei N, Franklin RJ (2003) Quantifying the early stages of remyelination following cuprizone-induced demyelination. Brain Pathol (Zurich, Switzerland) 13:329–339

Werneburg S, Fuchs HLS, Albers I, Burkhardt H, Gudi V, Skripuletz T, Stangel M, Gerardy-Schahn R, Hildebrandt H (2017) Polysialylation at early stages of oligodendrocyte differentiation promotes myelin repair. J Neurosci 37:8131–8141. https://doi.org/10.1523/jneurosci.1147-17.2017

Springer

9. Literaturverzeichnis

1. Kipp, M., et al., *Multiple sclerosis animal models: a clinical and histopathological perspective.* Brain Pathol, 2017. **27**(2): p. 123-137.
2. Duncan, G.J., et al., *Myelin regulatory factor drives remyelination in multiple sclerosis.* Acta Neuropathol, 2017. **134**(3): p. 403-422.
3. Thompson, A.J., et al., *Diagnosis of multiple sclerosis: 2017 revisions of the McDonald criteria.* Lancet Neurol, 2018. **17**(2): p. 162-173.
4. Noseworthy, J.H., et al., *Multiple sclerosis.* N Engl J Med, 2000. **343**(13): p. 938-52.
5. Frischer, J.M., et al., *The relation between inflammation and neurodegeneration in multiple sclerosis brains.* Brain, 2009. **132**(Pt 5): p. 1175-89.
6. Skripuletz, T., et al., *Astrocytes regulate myelin clearance through recruitment of microglia during cuprizone-induced demyelination.* Brain, 2013. **136**(Pt 1): p. 147-67.
7. Ransohoff, R.M. and V.H. Perry, *Microglial physiology: unique stimuli, specialized responses.* Annu Rev Immunol, 2009. **27**: p. 119-45.
8. Kettenmann, H., et al., *Physiology of microglia.* Physiol Rev, 2011. **91**(2): p. 461-553.
9. Bauer, J., et al., *Phagocytic activity of macrophages and microglial cells during the course of acute and chronic relapsing experimental autoimmune encephalomyelitis.* J Neurosci Res, 1994. **38**(4): p. 365-75.
10. Hooker, J.M. and R.E. Carson, *Human Positron Emission Tomography Neuroimaging.* Annu Rev Biomed Eng, 2019. **21**: p. 551-581.
11. Shoshan-Barmatz, V., S. Pittala, and D. Mizrachi, *VDAC1 and the TSPO: Expression, Interactions, and Associated Functions in Health and Disease States.* Int J Mol Sci, 2019. **20**(13).
12. Denora, N. and G. Natile, *An Updated View of Translocator Protein (TSPO).* Int J Mol Sci, 2017. **18**(12).
13. McNeela, A.M., et al., *TSPO regulation in reactive gliotic diseases.* J Neurosci Res, 2018. **96**(6): p. 978-988.
14. Cosenza-Nashat, M., et al., *Expression of the translocator protein of 18 kDa by microglia, macrophages and astrocytes based on immunohistochemical localization in abnormal human brain.* Neuropathol Appl Neurobiol, 2009. **35**(3): p. 306-28.
15. Chen, M.K., et al., *Peripheral benzodiazepine receptor imaging in CNS demyelination: functional implications of anatomical and cellular localization.* Brain, 2004. **127**(Pt 6): p. 1379-92.
16. Maeda, J., et al., *Phase-dependent roles of reactive microglia and astrocytes in nervous system injury as delineated by imaging of peripheral benzodiazepine receptor.* Brain Res, 2007. **1157**: p. 100-11.
17. Best, L., et al., *New and Old TSPO PET Radioligands for Imaging Brain Microglial Activation in Neurodegenerative Disease.* Curr Neurol Neurosci Rep, 2019. **19**(5): p. 24.
18. Hagens, M., B. van Berckel, and F. Barkhof, *Novel MRI and PET markers of neuroinflammation in multiple sclerosis.* Curr Opin Neurol, 2016. **29**(3): p. 229-36.
19. Dickens, A.M., et al., *Detection of microglial activation in an acute model of neuroinflammation using PET and radiotracers 11C-(R)-PK11195 and 18F-GE-180.* J Nucl Med, 2014. **55**(3): p. 466-72.
20. Unterrainer, M., et al., *TSPO PET with [(18)F]GE-180 sensitively detects focal neuroinflammation in patients with relapsing-remitting multiple sclerosis.* Eur J Nucl Med Mol Imaging, 2018. **45**(8): p. 1423-1431.

21.   Kaddatz, H., et al., *Cuprizone-induced demyelination triggers a CD8-pronounced T cell recruitment.* Glia, 2020.

22.   Praet, J., et al., *Cellular and molecular neuropathology of the cuprizone mouse model: clinical relevance for multiple sclerosis.* Neurosci Biobehav Rev, 2014. **47**: p. 485-505.

23.   Bakker, D.A. and S.K. Ludwin, *Blood-brain barrier permeability during Cuprizone-induced demyelination. Implications for the pathogenesis of immune-mediated demyelinating diseases.* J Neurol Sci, 1987. **78**(2): p. 125-37.

24.   Carlton, W.W., *Response of mice to the chelating agents sodium diethyldithiocarbamate, alpha-benzoinoxime, and biscyclohexanone oxaldihydrazone.* Toxicol Appl Pharmacol, 1966. **8**(3): p. 512-21.

25.   Hiremath, M.M., et al., *Microglial/macrophage accumulation during cuprizone-induced demyelination in C57BL/6 mice.* J Neuroimmunol, 1998. **92**(1-2): p. 38-49.

26.   Kipp, M., et al., *The cuprizone animal model: new insights into an old story.* Acta Neuropathol, 2009. **118**(6): p. 723-36.

27.   Constantinescu, C.S., et al., *Experimental autoimmune encephalomyelitis (EAE) as a model for multiple sclerosis (MS).* Br J Pharmacol, 2011. **164**(4): p. 1079-106.

28.   Bittner, S., et al., *Myelin oligodendrocyte glycoprotein (MOG35-55) induced experimental autoimmune encephalomyelitis (EAE) in C57BL/6 mice.* J Vis Exp, 2014(86).

29.   Acs, P. and B. Kalman, *Pathogenesis of multiple sclerosis: what can we learn from the cuprizone model.* Methods Mol Biol, 2012. **900**: p. 403-31.

30.   Ben-Nun, A., et al., *From classic to spontaneous and humanized models of multiple sclerosis: impact on understanding pathogenesis and drug development.* J Autoimmun, 2014. **54**: p. 33-50.

31.   Wagenknecht, N., et al., *Thalamus Degeneration and Inflammation in Two Distinct Multiple Sclerosis Animal Models.* J Mol Neurosci, 2016. **60**(1): p. 102-14.

32.   Scheld, M., et al., *Neurodegeneration Triggers Peripheral Immune Cell Recruitment into the Forebrain.* J Neurosci, 2016. **36**(4): p. 1410-5.

33.   Rüther, B.J., et al., *Combination of cuprizone and experimental autoimmune encephalomyelitis to study inflammatory brain lesion formation and progression.* Glia, 2017. **65**(12): p. 1900-1913.

34.   Nack, A., et al., *Expression of Translocator Protein and [18F]-GE180 Ligand Uptake in Multiple Sclerosis Animal Models.* Cells, 2019. **8**(2).

35.   Chrzanowski, U., et al., *Evaluation strategy to determine reliable demyelination in the cuprizone model.* Metab Brain Dis, 2019. **34**(2): p. 681-685.

10. Danksagung